BILINGUAL PUBLISHING GROUP

Journal of Electronic & Information Systems

Volume 6 • Issue 1 • April 2024 ISSN 2661-3204 (Online)

Volume 6 Issue 1 • April 2024 • ISSN 2661-3204 (Online)

Journal of Electronic & Information Systems

Editor-in-Chief

Associate Professor Xinggang Yan

BILINGUAL PUBLISHING GROUP

BILINGUAL PUBLISHING GROUP

Volume 6 | Issue 1 | April 2024 | Page1-38
Journal of Electronic & Information Systems

Contents

Articles

BILINGUAL PUBLISHING GROUP

Journal of Electronic & Information Systems

https://journals.bilpubgroup.com/index.php/jeis

ARTICLE

Sliding Mode-Based Distributed Trajectory Tracking Control of Four-body Train Systems

Yueheng Ding [*], ***Xinggang Yan***

School of Engineering, University of Kent, Canterbury, CT2 7NT, United Kingdom

ABSTRACT

This paper considers the speed tracking of a four-body train system modelled mathematically based on Newton's second law, which is described by a large-scale interconnected system with four subsystems. Uncertainties are included in the systems to represent the potential impacts on system performance caused by mechanical wear and external environmental changes. An adaptive sliding mode technique is employed to design a distributed control scheme to guarantee tracking accuracy. Coordinate transformations are introduced to transfer the model of train systems to a system in regular form to facilitate the design of the hyperplane and controllers. The *Barbashin-Krasovskii* theorem is employed to show the reachability of the hyperplane. In simulations, the Gaussian function is chosen as the desired signal, representing time-varying characteristics relevant to real-world situations, and the result demonstrates the feasibility of the proposed control strategy.

Keywords: Adaptive control; Distributed control; Large-scale interconnected systems; Sliding mode control; Trajectory tracking

1. Introduction

The train system, an integral part of the global transportation infrastructure, has played a pivotal role in shaping the socio-economic landscapes of nations worldwide. Offering a blend of efficiency, environmental sustainability, and unparalleled connectivity, rail transportation has not only bridged distant geographies but has also fostered economic growth, mitigated urban congestion, and introduced a greener mode of transit. Consequently, the study of such systems has received significant attention,

*CORRESPONDING AUTHOR:
Yueheng Ding, School of Engineering, University of Kent, Canterbury, CT2 7NT, United Kingdom; Email: ingyueheng@126.com

ARTICLE INFO
Received: 11 November 2023 | Revised: 2 January 2024 | Accepted: 16 January 2024 | Published Online: 25 January 2024
DOI: https://doi.org/10.30564/jeis.v6i1.6077

CITATION
Ding, Y.H., Yan, X.G., 2024. Sliding Mode Based Distributed Trajectory Tracking Control of Four-body Train Systems. Journal of Electronic & Information Systems. 6(1): 1–9. DOI: https://doi.org/10.30564/jeis.v6i1.6077

leading to numerous research findings [1–3].

Due to its unique construction, train systems can be described as a type of large-scale system that consists of a collection of interconnected lower-dimensional subsystems, where the behaviour of each subsystem is influenced by the interactions with other adjacent subsystems. Decentralised control, as a popular approach for interconnected systems, involves decomposing, if required, the system into smaller subsystems and designing local controllers for each subsystem independently [4,5]. In this approach, each subsystem's local controller is responsible for regulating its own behaviour while interacting and collaborating with neighbouring subsystems to achieve a global control objective. However, the train systems considered in this paper exhibit a distinctive chain structure, where the interconnections between subsystems can be modelled as functions of their own states and adjacent system states only. In such cases, the distributed scheme allows the local sub-controller to utilise not only information from its own subsystem but also information from its neighbouring subsystems, like information from adjacent subsystems. This characteristic aligns well with the interconnected nature of the train system studied in this paper. Therefore, the use of distributed control is a natural choice [6,7] and serves as the motivation for employing distributed control techniques in this paper.

Tracking control is a crucial subject in both control theory and control engineering, and significant progress has been made in this field (refer to the works [8,9]). In the work [10], an adaptive fuzzy technique-based tracking control approach for interconnected systems is investigated, while the work [11] focuses on decentralised tracking control for large-scale systems, exploring model reference control. However, it is important to note that the findings, obtained in works [10,11], impose a relatively strong limitation on the structural characteristics of the studied system. This specific system structure deviates somewhat from real-world scenarios. Therefore, investigating a more general and realistic train model is a research direction that holds significant value, and it aligns with the problem addressed in this paper. Furthermore, the sliding mode technique is often employed to enhance the robustness of interconnected systems with uncertainties, as the sliding mode dynamics typically govern system performance without uncertainties [12]. Hence, sliding mode control-based methods have been extensively applied in system tracking control. In the work [13], a tracking problem for a class of large-scale systems with interconnections is addressed using sliding mode techniques, which require that the desired signals are constant.

Therefore, this paper focuses on a distributed control approach using sliding mode techniques to tackle the speed tracking challenge of a four-body train system where some extensions and improvements of the time-varying desired signals and unknown interconnections are explored. According to the prior works [14,15], the train system is modelled as an interconnected system with unknown uncertainties and disturbances. Then, a sliding surface is synthesised based on the tracking and the *Barbashin-Krasovskii* theorem is introduced to guarantee the occurrence of a reaching phase and sliding motion with the proposed distributed control. The main contributions of this paper are listed as follows.

- Through the application of sliding mode techniques, the strong robustness of the four-body train system can be guaranteed, due to the sliding motion is insensitive [12] to matched uncertainty and disturbance.
- In comparison to the existing result [16], the desired reference signal is permitted to have a more general form, specifically, a smooth function, and is no longer restricted to be constant.
- Asymptotically tracking the performance of the system with unknown uncertainties is achieved with the proposed control scheme, which involves the use of adaptive techniques.

Lastly, a simulation is conducted to demonstrate the effectiveness of the proposed approaches.

2. System description

According to the work [17], the train system, as depicted in **Figure 1**, can be represented mathematically as:

$$M_i \ddot{z}_i(t) = F_i(t) + F_{i-1}(t) - F_{i+1}(t) - F_{r_i}(t) \tag{1}$$

for $i = 1, 2, 3, 4$, where M_i represents the mass of the ith body, $\ddot{z}_i$ *is* the corresponding acceleration, and F_i *is* the traction force. Additionally, F_{i-1} and F_{i+1} are the restoring forces caused by adjacent bodies. $F_r i$ denotes the resistive force.

Remark 1: Equation (1) describes the most general situation (the middle bodies). For the special parts, like the locomotive and caboose, some terms in (1) will be omitted due to the real situation, which will be discussed later.

Due to the relatively small displacements between bodies, the restoring force can be modelled approximately as the following linear function:

$$F_{i+1}(t) = k_i(z_i - z_{i+1}) + d_i(\dot{z}_i - \dot{z}_{i+1}) \tag{2}$$

where k_i and d_i represent the spring and damping parameters, respectively. z_i, z_{i+1}, $\dot{z}_i$, and $\dot{z}_i+1$ correspond to the ith and $(i + 1)$th displacements and corresponding speeds, respectively for $i = 1, 2, 3, 4$. The general resistance $F_r i(t)$ can be modelled by (see the works [18–20]):

$$F_{r_i}(t) = \begin{cases} b_{1o} + b_{1v}\dot{z}_1 + b_{1a}\dot{z}_1^2, & i = 1 \\ b_{io} + b_{iv}\dot{z}_i, & i = 2,3,4 \end{cases} \tag{3}$$

where b_{io} , b_{iv} and b_{1a} are the resistance coefficients. $b_{1a}\dot{z}_1^2$ denotes aerodynamic drag, while b_{io} and $b_{iv}\dot{z}_i$ are rolling mechanical resistances.

From (1)–(3), the four-body train system in **Figure 1** is given by:

$$\begin{aligned} M_1\ddot{z}_1 = {} & F_1 - (k_1 + \Delta k_1)(z_1 - z_2) - (d_1 + \Delta d_1)(\dot{z}_1 - \dot{z}_2) \\ & - b_{1o} - b_{1v}\dot{z}_1 - b_{1a}\dot{z}_1^2, \end{aligned} \tag{4}$$

$$\begin{aligned} M_i\ddot{z}_i = {} & F_i - (k_i + \Delta k_i)(z_i - z_{i+1}) - (k_{i-1} + \Delta k_{i-1})(z_i - z_{i-1}) \\ & - (d_i + \Delta d_i)(\dot{z}_i - \dot{z}_{i+1}) - (d_{i-1} + \Delta d_{i-1})(\dot{z}_i - \dot{z}_{i-1}) \\ & - b_{io} - b_{iv}\dot{z}_i, \ i = 2,3 \end{aligned} \tag{5}$$

$$\begin{aligned} M_4\ddot{z}_4 = {} & F_4 - (k_3 + \Delta k_3)(z_4 - z_3) - (d_3 + \Delta d_3)(\dot{z}_4 - \dot{z}_3) \\ & - b_{4o} - b_{4v}\dot{z}_4, \end{aligned} \tag{6}$$

where Δk_i and Δd_i for $i = 1, 2, 3$ are unknown constants. $\dot{z}_1$, $\dot{z}_2$, $\dot{z}_3$ and $\dot{z}_4$ are taken as the system's outputs.

Remark 2: In this paper, a more realistic situation is taken into account. It is assumed that there are variations in the spring and damping parameters, denoted by Δk_i and Δd_i, respectively, in the interconnections compared with their nominal values. These variations may occur due to aging of components and external factors such as temperature changes, external disturbances, and other similar influences.

3. System structure analysis

For the four-body train described in system (4)–(6), choose the following coordinate transformation:

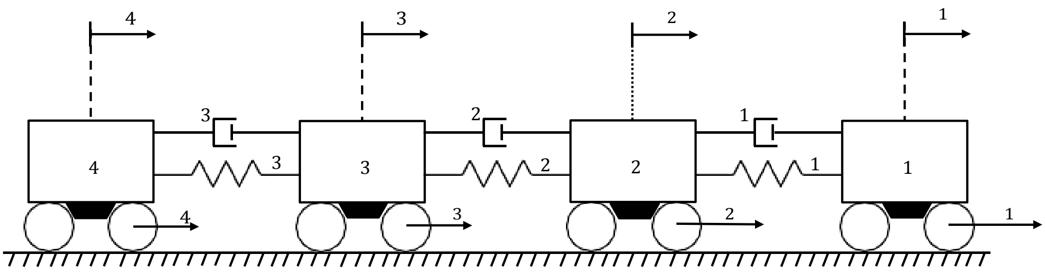

Figure 1. Sketch of a four-body train system.

$$\begin{bmatrix} x_{11} \, x_{12} \, x_{21} \, x_{22} \, x_{31} \, x_{32} \, x_{41} \, x_{42} \end{bmatrix}^T = \begin{bmatrix} z_1 \, \dot{z}_1 \, z_2 \, \dot{z}_2 \, z_3 \, \dot{z}_3 \, z_4 \, \dot{z}_4 \end{bmatrix}^T \tag{7}$$

Furthermore, an additional feedback transformation is introduced:

$$F_1 = k_1(x_{11} - x_{21}) + d_1(x_{12} - x_{22}) + b_{1o} + b_{1v}x_{12} + b_{1a}x_{12}^2 + M_1 v_1, \tag{8}$$

$$F_i = k_i(x_{i,1} - x_{i+1,1}) + k_{i-1}(x_{i,1} - x_{i-1,1}) + d_i(x_{i,2} - x_{i+1,2}) + d_{i-1}(x_{i,2} - x_{i-1,2}) + b_{io} + b_{iv}x_{i,2} + M_i v_i, \quad i = 2,3 \tag{9}$$

$$F_4 = k_3(x_{41} - x_{31}) + d_3(x_{42} - x_{32}) + b_{4o} + b_{4v}x_{42} + M_4 v_4, \tag{10}$$

where v_1, v_2, v_3 and v_4 are the new control inputs which will be designed later. In the new coordinates $x = col(x_{11}, x_{12}, \ldots, x_{42})$, system (4)–(6) can be described by:

$$\dot{x}_{i1} = x_{i2} \tag{11}$$

$$\dot{x}_{i2} = v_i + H_i(x), \quad i = 1,2,3,4 \tag{12}$$

where

$$H_1(x) = -\frac{\Delta k_1}{M_1}(x_{11} - x_{21}) - \frac{\Delta d_1}{M_1}(x_{12} - x_{22}), \tag{13}$$

$$H_i(x) = -\frac{\Delta k_i}{M_i}(x_{i,1} - x_{i+1,1}) - \frac{\Delta k_{i-1}}{M_i}(x_{i,1} - x_{i-1,1}) - \frac{\Delta d_i}{M_i}(x_{i,2} - x_{i+1,2}) - \frac{\Delta d_{i-1}}{M_i}(x_{i,2} - x_{i-1,2}), \quad i = 2,3 \tag{14}$$

$$H_4(x) = -\frac{\Delta k_3}{M_4}(x_{41} - x_{31}) - \frac{\Delta d_3}{M_4}(x_{42} - x_{32}), \tag{15}$$

where $H_i(x)$ represents uncertainties in the interconnections of the ith subsystems for $i = 1, 2, 3, 4$ with the state $x = col(x_{11}, x_{12}, x_{21}, x_{22}, x_{31}, x_{32}, x_{41}, x_{42}) \in R^8$. The inputs $v_i \in R$.

Remark 3: According to (13)–(15), the interconnected uncertainties $H_i(x)$ in the ith subsystem are functions of the unknown coefficients, state x_i and its adjacent states x_{i-1} and x_{i+1}. The state $x_i = col(x_{i1}, x_{i2})$ for $i = 1, 2, 3, 4$. It is clear to see that the interconnected structure in (13)–(15) reflects the practical train system shown in **Figure 1**. Therefore, distributed control is naturally considered to cope with the tracking problem of the system above.

Consider the interconnected system (11)–(12) with interconnections in (13)–(15). The desired displacement of each body in the train system is assumed as $S_d(t)$. Its first derivate is thus the desired signal $y_d(t)$ (speed signal). Then, the objective of this paper is to design an adaptive-based distributed sliding mode control that allows the speed of each body to track the desired signal $y_d(t)$. In other words, the objective of this paper is to achieve $\lim_{t\to\infty} |y_d(t) - x_{i2}(t)| = 0$ for $i = 1, 2, 3, 4$. Additionally, the displacement errors between the desired displacement $S_d(t)$ and the actual displacement of the four bodies should remain to be bounded, despite the presence of unknown uncertainties in the interconnections.

Remark 4: It is important to note that the displacement states z_1, z_2, z_3, and z_4 may tend towards infinity as time t approaches infinity, especially when the speeds are non-zero. However, from a practical perspective, it is essential to ensure that the displacement errors $S_d(t) - z_1$, $S_d(t) - z_2$, $S_d(t) - z_3$, and $S_d(t) - z_4$ remain bounded. Failure to do so may result in the connections between adjacent bodies being broken.

Assumption 3.1: The desired signal $y_d(t)$ and its first derivate $\dot{y}_d(t)$ are assumed to be smooth for all $t \in [0, \infty)$. In this case, a proper transformation $T = diag\{T_i\}$ for $i = 1, 2, 3, 4$ with T_i is defined by:

$$T_i \triangleq \begin{bmatrix} \delta_i(t) \\ e_i(t) \end{bmatrix} = \begin{bmatrix} S_d(t) - x_{i1}(t) \\ y_d(t) - x_{i2}(t) \end{bmatrix} \tag{16}$$

where $S_d(t)$ and $y_d(t)$ satisfy the Assumption 3.1.

Then, system (11)–(12) in the new coordinates $col(\delta_i, e_i)$ can be described by:

$$\dot{\delta}_i(t) = e_i(t), \tag{17}$$

$$\dot{e}_i(t) = \dot{y}_d(t) - v_i + \Gamma_i(\delta, e), \quad i = 1,2,3,4 \tag{18}$$

where $\delta = col(\delta_1, \delta_2, \delta_3, \delta_4)$, $e = col(e1, e2, e3, e4)$ and

$$\Gamma_1(\delta, e) = T_1 H_1(x)|_{x=T^{-1}col(\delta,e)} = \alpha_1(\delta_2 - \delta_1) + \beta_1(e_2 - e_1), \tag{19}$$

$$\begin{aligned}\Gamma_i(\delta, e) = T_i H_i(x)|_{x=T^{-1}col(\delta,e)} &= \alpha_{i1}(\delta_{i+1} - \delta_i) + \alpha_{i2}(\delta_{i-1} - \delta_i)\\ &+ \beta_{i1}(e_{i+1} - e_i) + \beta_{i2}(e_{i-1} - e_i), \ i = 2,3\end{aligned} \tag{20}$$

$$\Gamma_4(\delta, e) = T_4 H_4(x)|_{x=T^{-1}col(\delta,e)} = \alpha_4(\delta_3 - \delta_4) + \beta_4(e_3 - e_4), \tag{21}$$

with

$$\alpha_1 = \frac{\Delta k_1}{M_1}, \beta_1 = \frac{\Delta d_1}{M_1}, \alpha_{i1} = \frac{\Delta k_i}{M_i}, \alpha_{i2} = \frac{\Delta k_{i-1}}{M_1}, \beta_{i1} = \frac{\Delta d_i}{M_i},$$
$$\beta_{i2} = \frac{\Delta d_{i-1}}{M_i}, (i = 2,3), \alpha_4 = \frac{\Delta k_3}{M_4} \quad \text{and} \quad \beta_4 = \frac{\Delta d_3}{M_4}.$$

4. Stability analysis and control law construction

4.1 Stability analysis of sliding motion

For system (17)–(18), consider the sliding surface defined by:

$$col(e_1, e_2, e_3, e_4) = 0. \tag{22}$$

From the sliding mode control theory, the sliding motion of the system (17)–(18) corresponding to the sliding surface (22) is given by:

$$\dot{\delta}_i(t) = 0. \ i = 1,2,3,4 \tag{23}$$

It is easy to see from (23) that $\delta_i(t)$ for $i = 1, 2, 3, 4$ are bounded when the sliding motion occurs, which is consistent with the objective of this paper.

4.2 Reachability problem and distributed control design

This section aims to design a distributed sliding mode control to drive the system into the sliding surface (22). Then, the controllers are proposed as:

$$v_1 = \dot{y}_d(t) + \hat{\alpha}_1(t)(\delta_2 - \delta_1) + \hat{\beta}_1(t)(e_2 - e_1) + k_1 e_1, \tag{24}$$

$$\begin{aligned}v_i = \dot{y}_d(t) &+ \hat{\alpha}_{i1}(t)(\delta_{i+1} - \delta_i) + \hat{\alpha}_{i2}(t)(\delta_{i-1} - \delta_i) + \hat{\beta}_{i1}(t)(e_{i+1} - e_i)\\ &+ \hat{\beta}_{i2}(t)(e_{i-1} - e_i) + k_i e_i, \ i = 2,3\end{aligned} \tag{25}$$

$$v_4 = \dot{y}_d(t) + \hat{\alpha}_4(t)(\delta_3 - \delta_4) + \hat{\beta}_4(t)(e_3 - e_4) + k_4 e_4, \tag{26}$$

where k_i for $i = 1, 2, 3, 4$ are positive constants. $\alpha\hat{}_1(t)$, $\hat{\beta}1(t)$, $\alpha\hat{}_{i1}(t)$, $\alpha\hat{}_{i2}(t)$, $\hat{\beta}i1(t)$, $\hat{\beta}i2(t)$, $(i = 2, 3)$, $\alpha\hat{}_4(t)$ and $\hat{\beta}4(t)$ are the approximation to the parameters α_1, β_1, α_{i1}, α_{i2}, β_{i1}, β_{i2}, $(i = 2, 3)$, α_4 and β_4 in (19)–(21) respectively, and the adaptive laws are given by:

$$\begin{aligned}&\alpha\dot{\hat{}}_1(t) = e_1(\delta_2 - \delta_1),\\ &\hat{\beta}1(t) = e1(e2 - e1);\end{aligned} \tag{27}$$

$$\begin{aligned}&\alpha\dot{\hat{}}_{i1}(t) = e_i(\delta_{i+1} - \delta_i), \ \alpha\dot{\hat{}}i2(t) = e_i(\delta_{i-1} - \delta_i),\\ &\hat{\beta}i1(t) = ei(ei+1 - ei), \ \hat{\beta}i2(t) = ei(ei-1 - ei); i = 2, 3\end{aligned} \tag{28}$$

$$\begin{aligned}&\alpha\dot{\hat{}}_4(t) = e_4(\delta_3 - \delta_4),\\ &\hat{\beta}4(t) = e4(e3 - e4).\end{aligned} \tag{29}$$

Remark 5: From (8)–(10), the final distributed controller in the original coordinate is given by:

$$\begin{aligned}F_1 = &(k_1 + M_1\hat{\alpha}_1(t))(x_{11} - x_{21}) + (d_1 + M_1\hat{\beta}_1(t))(x_{12} - x_{22})\\ &+ b_{1o} + (b_{1v} - M_1 k_1)x_{12} + b_{1a}x_{12}^2\\ &+ M_1(\dot{y}_d(t) + k_1 y_d),\end{aligned} \tag{30}$$

$$\begin{aligned}F_i = &(k_i + M_i\hat{\alpha}_{i1}(t))(x_{i,1} - x_{i+1,1}) + (k_{i-1} + M_i\hat{\alpha}_{i2}(t))\\ &(x_{i,1} - x_{i-1,1}) + (d_i + M_i\hat{\beta}_{i1}(t))(x_{i,2} - x_{i+1,2})\\ &+ (d_{i-1} + M_i\hat{\beta}_{i2}(t))(x_{i,2} - x_{i-1,2})\\ &+ b_{io} + (b_{iv} - M_i k_i)x_{i,2} + M_i(\dot{y}_d(t) + k_i y_d), \ i = 2,3\end{aligned} \tag{31}$$

$$F_4 = (k_3 + M_4\hat{\alpha}_4(t))(x_{41} - x_{31}) + (d_3 + M_4\hat{\beta}_4(t)) (x_{42} - x_{32}) + b_{4o} + (b_{4v} - M_4 k_4)x_{42} + M_4(\dot{y}_d(t) + k_4 y_d). \tag{32}$$

with the parameters $\hat{\alpha}_1(t)$, $\hat{\beta}1(t)$, $\hat{\alpha}_{i1}(t)$, $\hat{\alpha}_{i2}(t)$, $\hat{\beta}i1(t)$, $\hat{\beta}i2$, $(i = 2, 3)$, $\hat{\alpha}_4(t)$ and $\hat{\beta}4(t)$ satisfies (27)–(29).

Theorem 1: For the interconnected system (17)–(18) with the adaptive laws in (27)–(29), under Assumption 3.1, the controller (24)–(26) can drive the considered system to the sliding surface (22) and maintains a sliding motion on it thereafter.

Proof 1: Define the adaptive errors as:

$$\tilde{\alpha}_1(t) = \alpha_1 - \hat{\alpha}_1(t), \ \ \tilde{\beta}_1(t) = \beta_1 - \hat{\beta}_1(t); \tag{33}$$

$$\begin{aligned}&\tilde{\alpha}_{i1}(t) = \alpha_{i1} - \hat{\alpha}_{i1}(t), \ \ \tilde{\alpha}_{i2}(t) = \alpha_{i2} - \hat{\alpha}_{i2}(t),\\ &\tilde{\beta}_{i1}(t) = \beta_{i1} - \hat{\beta}_{i1}(t), \ \ \tilde{\beta}_{i2}(t) = \beta_{i2} - \hat{\beta}_{i2}(t); \quad i = 2,3\end{aligned} \tag{34}$$

$$\tilde{\alpha}_4(t) = \alpha_4 - \hat{\alpha}_4(t), \ \ \tilde{\beta}_4(t) = \beta_4 - \hat{\beta}_4(t). \tag{35}$$

Choose a Lyapunov candidate function as:

$$\begin{aligned}V &= \frac{1}{2}\sum_{i=1}^{4} e_i^2 + \frac{1}{2}\sum_{i=2}^{3}(\tilde{\alpha}_{i1}^2 + \tilde{\alpha}_{i2}^2 + \tilde{\beta}_{i1}^2 + \tilde{\beta}_{i2}^2)\\ &+ \frac{1}{2}(\tilde{\alpha}_1^2 + \tilde{\beta}_1^2 + \tilde{\alpha}_4^2 + \tilde{\beta}_4^2).\end{aligned} \tag{36}$$

Then, the time derivate of V along the trajectories of (18) is given by:

$$\begin{aligned}\dot{V} &= \sum_{i=1}^{4} e_i\dot{e}_i - \sum_{i=2}^{3}(\tilde{\alpha}_{i1}\dot{\hat{\alpha}}_{i1} + \tilde{\alpha}_{i2}\dot{\hat{\alpha}}_{i2} + \tilde{\beta}_{i1}\dot{\hat{\beta}}_{i1} + \tilde{\beta}_{i2}\dot{\hat{\beta}}_{i2})\\ &- \tilde{\alpha}_1\dot{\hat{\alpha}}_1 - \tilde{\beta}_1\dot{\hat{\beta}}_1 - \tilde{\alpha}_4\dot{\hat{\alpha}}_4 - \tilde{\beta}_4\dot{\hat{\beta}}_4\\ &= -\sum_{i=1}^{4} k_i e_i^2 + \sum_{i=2}^{3}(e_i(\tilde{\alpha}_{i1}(\delta_{i+1} - \delta_i) + \tilde{\alpha}_{i2}(\delta_{i-1} - \delta_i)\\ &+ \tilde{\beta}_{i1}(e_{i+1} - e_i) + \tilde{\beta}_{i2}(e_{i-1} - e_i)) - \tilde{\alpha}_{i1}\dot{\hat{\alpha}}_{i1} - \tilde{\alpha}_{i2}\dot{\hat{\alpha}}_{i2} - \tilde{\beta}_{i1}\dot{\hat{\beta}}_{i1} - \tilde{\beta}_{i2}\dot{\hat{\beta}}_{i2})\\ &+ e_1(\tilde{\alpha}_1(\delta_2 - \delta_1) + \tilde{\beta}_1(e_2 - e_1)) - \tilde{\alpha}_1\dot{\hat{\alpha}}_1 - \tilde{\beta}_1\dot{\hat{\beta}}_1 + e_4(\tilde{\alpha}_4(\delta_3 - \delta_4)\\ &+ \tilde{\beta}_4(e_3 - e_4)) - \tilde{\alpha}_4\dot{\hat{\alpha}}_4 - \tilde{\beta}_4\dot{\hat{\beta}}_4\\ &= -\sum_{i=1}^{4} k_i e_i^2.\end{aligned} \tag{37}$$

From the analysis above, $\dot{V}$ is a negative semi-definite function. Then, from the *Barbashin-Krasovskii* theorem (refer to section 4.2 in the work [21]), its solution $e_i(t) \to 0$ as $t \to \infty$ for $i = 1, 2, 3, 4$. Therefore, the proposed controller (24)–(26) can drive the system to the sliding surface. By integrating (27)–(29) and considering the results $\lim_{t\to\infty} e_i(t) = 0$, it is evident that the adaptive parameters $\hat{\alpha}_1(t)$, $\hat{\beta}1(t)$, $\hat{\alpha}_{i1}(t)$, $\hat{\alpha}_{i2}(t)$, $\hat{\beta}i1(t)$, $\hat{\beta}i2(t)$, (for $i = 2, 3$), $\hat{\alpha}_4(t)$ and $\hat{\beta}4(t)$ are bounded. Hence, the result is valid.

Remark 6: The boundedness of the sliding motion (23) is demonstrated. Theorem 1 illustrates that the control scheme (24)–(26) can drive system (17)–(18) to the sliding surface (22). According to sliding mode theory, this implies that the proposed distributed control approach (30)–(32) not only ensures that each body's speed asymptotically tracks the desired signal $y_d(t)$ but also guarantees that all displacement errors between adjacent bodies remain bounded.

Remark 7: The adaptive laws (27)–(29) proposed above ensure the estimation of parameters rather than their identification. This implies that the adaptive parameters may not converge to their true values. Only the boundedness of the parameters' estimation is guaranteed in this paper.

5. Simulation study

In this section, a simulation is conducted to demonstrate the obtained results. For the simulation purpose, the following generalized Gaussian distribution depicted in **Figure 2** from the works [22,23] is chosen as the desired speed signal.

$$y_d(t) = \frac{6}{\Gamma(\frac{1}{6})} \cdot e^{-(\frac{|t-10|}{5})^6}, \ \ t \geq 0 \tag{38}$$

where $\Gamma(\cdot)$ denotes the Gamma function. This signal is consistent with the practical train system running between two stations.

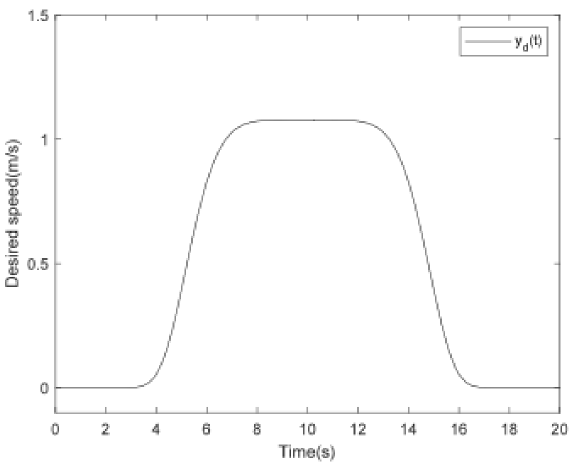

Figure 2. Time responses of the desired signal.

The nominal parameters of all bodies are set as:

$M_1 = M_2 = M_3 = M_4 = 126000\ kg,$
$d_1 = d_2 = d_3 = 80 \times 10^4\ Ns/m,$
$k_1 = k_2 = k_3 = 100 \times 10^6\ N/m,$
$b_{1o} = b_{2o} = b_{3o} = b_{4o} = 6.362 \times 10^{-3}\ N/kg,$
$b_{1v} = b_{2v} = b_{3v} = b_{4v} = 1.08 \times 10^{-4}\ Ns/(mkg),$
$b_{1a} = 2.06 \times 10^{-5}\ Ns^2/(m^2kg).$

The initial condition is set as $[x_{11}, x_{12}, x_{21}, x_{22}, x_{31}, x_{32}, x_{41}, x_{42}]^\top = [0\ 0.8\ 0\ 0.5\ 0\ 0.2\ 0\ 0]^\top$. The controller gains are determined as $k_1 = 0.7$, $k_2 = 5$, $k_3 = 2$ and $k_4 = 1$.

With the distributed sliding mode control (DSMC) proposed in this paper, the speed of each body asymptotically tracks the desired signal $y_d(t)$, as illustrated by the blue line in **Figure 3**. For comparison, a robust distributed controller (DC) in the work [16] is also considered as shown by the red line in **Figure 3**. It can be observed that the controller using DSMC achieved rapid convergence within the first 5 seconds, while the controller using DC exhibited poorer tracking performance. Concurrently, the displacement errors $\delta_i(t)$ for $i = 1, 2, 3, 4$ remain stable, as shown in **Figure 4**. The adaptive parameters $\hat{\alpha}_1(t)$, $\hat{\beta}1(t)$, $\hat{\alpha}_{i1}(t)$, $\hat{\alpha}_{i2}(t)$, $\hat{\beta}i1(t)$, $\hat{\beta}i2(t)$, $(i = 2, 3)$, $\hat{\alpha}_4(t)$ and $\hat{\beta}4(t)$ are bounded, as demonstrated in **Figure 5**. The simulation results align with the theoretical findings, validating the proposed approach.

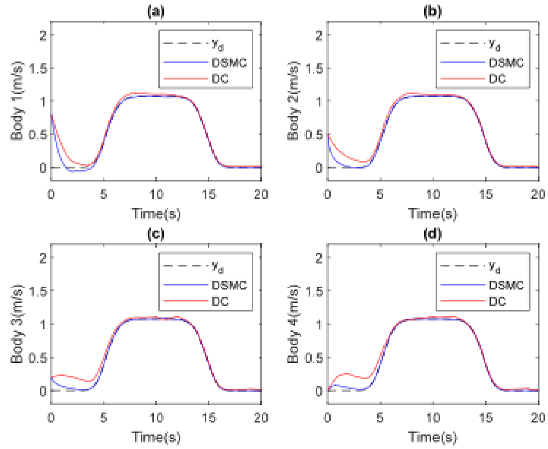

Figure 3. Tracking the performance of the system. (a). A comparative tracking results of the body 1. (b). A comparative tracking results of the body 2. (c). A comparative tracking results of the body 3. (d). A comparative tracking results of the body 4.

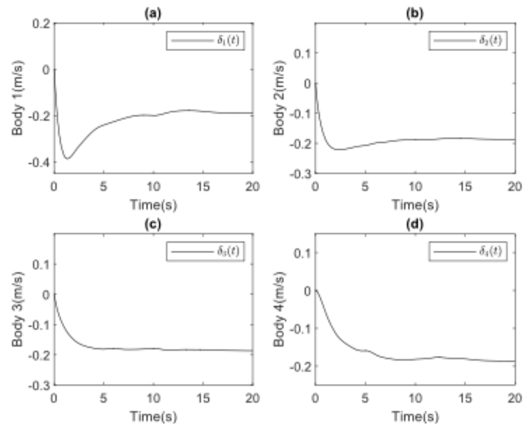

Figure 4. Displacement errors between the desired displacement S_d & the displacement of each body with DSMC. (a). Displacement error of the body 1. (b). Displacement error of the body 2. (c). Displacement error of the body 3. (d). Displacement error of the body 4.

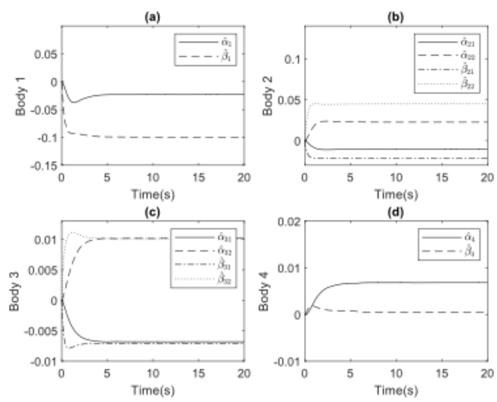

Figure 5. The time response of the estimated parameters. (a). Estimated parameters of the body 1. (b). Estimated parameters of the body 2. (c). Estimated parameters of the body 3. (d). Estimated parameters of the body 4.

6. Conclusions

This paper introduces a distributed tracking control method for a four-body train system with unknown uncertainties in its interconnections, leveraging sliding mode techniques. Unlike previous methods, our approach accommodates time-varying desired signals. The proposed distributed sliding mode control scheme based on the *Barbashin-Krasovskii* theorem has been proposed to fulfil the reachability condition, ensuring the reachability condition is met. Additionally, the unknown interconnections are approximated by using adaptive techniques. Simulation results for the four-body system validate the effectiveness and practicality of the proposed approach.

In the process of train control, the use of distributed control may lead to the entire system coming to a halt. For this, one of the advantages of decentralised control is that the controller of each subsystem only collects local information, meaning that even if other subsystems experience malfunctions, decentralised control can still ensure the normal operation of the entire system. Therefore, combining decentralised control with the tracking control of trains is a promising research direction.

Author Contributions

This paper has been researched and written by Yueheng Ding and Xinggang Yan.

Conflict of Interest

We declare that there is no conflict of interest regarding the publication of this paper.

References

[1] Zhao, L., Cai, B., Xu, J., et al., 2013. Study of the track-train continuous information transmission process in a high-speed railway. IEEE Transactions on Intelligent Transportation Systems. 15(1), 112–121. DOI: https://doi.org/10.1109/TITS.2013.2274617

[2] Lin, P., Huang, Y., Zhang, Q., et al., 2020. Distributed velocity and input constrained tracking control of high-speed train systems. IEEE Transactions on Systems, Man, and Cybernetics: Systems. 51(12), 7882–7888. DOI: https://doi.org/10.1109/TSMC.2020.2987339

[3] He, Y., Wu, J., Zheng, Y., et al., 2022. Track defect detection for high-speed maglev trains via deep learning. IEEE Transactions on Instrumentation and Measurement. 71, 1–8. DOI: https://doi.org/10.1109/TIM.2022.3151165

[4] Yan, X.G., Wang, J.J., Lu, X.Y., et al., 1998. Decentralized output feedback robust stabilization for a class of nonlinear interconnected systems with similarity. IEEE Transactions on Automatic Control. 43(2), 294–299. DOI: https://doi.org/10.1109/9.661085

[5] Yan, X.G., Xie, L., 2003. Reduced-order control for a class of nonlinear similar interconnected systems with mismatched uncertainty. Automatica. 39(1), 91–99. DOI: https://doi.org/10.1016/S0005-1098(02)00194-2

[6] Tan, L.N., 2018. Distributed H∞ optimal tracking control for strict-feedback nonlinear large-scale systems with disturbances and saturating actuators. IEEE Transactions on Systems, Man, and Cybernetics: Systems. 50(11), 4719–4731. DOI: https://doi.org/10.1109/TSMC.2018.2861470

[7] Zhang, D., Nguang, S.K., Yu, L., 2017. Distributed control of large-scale networked control systems with communication constraints and topology switching. IEEE Transactions on Systems, Man, and Cybernetics: Systems. 47(7), 1746–1757. DOI: https://doi.org/10.1109/TSMC.2017.2681702

[8] Cai, H., Hu, G., 2017. Distributed tracking control of an interconnected leader—follower multiagent system. IEEE Transactions on Automatic Control. 62(7), 3494–3501. DOI: https://doi.org/10.1109/TAC.2017.2660298

[9] Liu, C., Zhang, H., Xiao, G., et al., 2019. Integral reinforcement learning based decentralized optimal tracking control of unknown nonlinear

large-scale interconnected systems with constrained-input. Neurocomputing. 323, 1–11. DOI: https://doi.org/10.1016/j.neucom.2018.09.011

[10] Ren, X.X., Yang, G.H., Li, X.J., 2019. Global adaptive fuzzy distributed tracking control for interconnected nonlinear systems with communication constraints. IEEE Transactions on Fuzzy Systems. 28(2), 333–345. DOI: https://doi.org/10.1109/TFUZZ.2019.2905827

[11] Pagilla, P.R., Dwivedula, R.V., Siraskar, N.B., 2007. A decentralized model reference adaptive controller for large-scale systems. IEEE/ASME Transactions on Mechatronics. 12(2), 154–163. DOI: https://doi.org/10.1109/TMECH.2007.892823

[12] Yan, X.G., Spurgeon, S.K., Edwards, C., 2018. Variable structure control of complex systems analysis and design. Springer: Berlin.

[13] Zhu, G., Nie, L., Lv, Z., et al., 2020. Adaptive fuzzy dynamic surface sliding mode control of large-scale power systems with prescribe output tracking performance. ISA Transactions. 99, 305–321. DOI: https://doi.org/10.1016/j.isatra.2019.08.063

[14] Ding, Y.H, Yan, X.G., Mao, Z.H., et al. (editors), 2022. Sliding mode based decentralized tracking control of underactuated four-body systems. 2022 13th Asian Control Conference (ASCC); 2022 May 4–7; Jeju, Korea. New York: IEEE. p. 1765–1770. DOI: https://doi.org/10.23919/ASCC56756.2022.9828154

[15] Song, Q., Song, Y.D., Tang, T., et al., 2011. Computationally inexpensive tracking control of high-speed trains with traction/braking saturation. IEEE Transactions on Intelligent Transportation Systems. 12(4), 1116–1125. DOI: https://doi.org/10.1109/TITS.2011.2143409

[16] Wang, X., Zhu, L., Wang, H., et al., 2019. Robust distributed cruise control of multiple high-speed trains based on disturbance observer. IEEE Transactions on Intelligent Transportation Systems. 22(1), 267–279. DOI: https://doi.org/10.1109/TITS.2019.2956162

[17] Mao, Z., Tao, G., Jiang, B., et al., 2021. Zero dynamics analysis and adaptive tracking control of underactuated multibody systems with flexible links. International Journal of Control. 94(7), 1931–1943. DOI: https://doi.org/10.1080/00207179.2019.1686179

[18] Mao, Z., Tao, G., Jiang, B., et al., 2020. Adaptive control design and evaluation for multibody high-speed train dynamic models. IEEE Transactions on Control Systems Technology. 29(3), 1061–1074. DOI: https://doi.org/10.1109/TCST.2020.2991119

[19] Tang, H., Wang, Q., Feng, X., 2017. Robust stochastic control for high-speed trains with nonlinearity, parametric uncertainty, and multiple time-varying delays. IEEE Transactions on Intelligent Transportation Systems. 19(4), 1027–1037. DOI: https://doi.org/10.1109/TITS.2017.2710138

[20] Rochard, B.P., Schmid, F., 2000. A review of methods to measure and calculate train resistances. Proceedings of the Institution of Mechanical Engineers, Part F: Journal of Rail and Rapid Transit. 214(4), 185–199. DOI: https://doi.org/10.1243/0954409001531306

[21] Hassan, K.K., 2001. Nonlinear systems. Prentice Hall: Hoboken.

[22] Cui, S., Datcu, M., 2012. Statistical wavelet subband modeling for multi-temporal SAR change detection. IEEE Journal of Selected Topics in Applied Earth Observations and Remote Sensing. 5(4), 1095–1109. DOI: https://doi.org/10.1109/JSTARS.2012.2200655

[23] Mallat, S.G., 1989. A theory for multiresolution signal decomposition: The wavelet representation. IEEE Transactions on Pattern Analysis and Machine Intelligence. 11(7), 674–693. DOI: https://doi.org/10.1109/34.192463

BILINGUAL PUBLISHING GROUP

Journal of Electronic & Information Systems

https://journals.bilpubgroup.com/index.php/jeis

ARTICLE

Attribute-specific Cyberbullying Detection Using Artificial Intelligence

Adeyinka Orelaja[1*], *Chidubem Ejiofor*[2], *Samuel Sarpong*[3], *Success Imakuh*[4*], *Christian Bassey*[5], *Iheanyichukwu Opara*[6], *Josiah Nii Armah Tettey*[7], *Omolola Akinola*[8]

[1] *Department of Computer Science, Austin Peay State University, Tennessee, 37044, USA*
[2] *Department of Computer Science, Western Illinois University, Macomb, Illinois, 61455, USA*
[3] *Department of Computing, East Tennessee State University, Tennessee, 37604, USA*
[4] *Department of Computing, Teesside University, Middlesbrough, TS1 3BX, United Kingdom*
[5] *Department of Computer Science, Innopolis University, Innopolis, 420500, Russia*
[6] *Department of Oil and Gas Engineering, Robert Gordon University, Aberdeen, AB10 7AQ, United Kingdom*
[7] *Department of Computer Science, Wright State University, Dayton, Ohio, 45435, USA*
[8] *Department of Information System and Analysis, Lamar University, Beaumont, Texas, 77705, USA*

ABSTRACT

Cyberbullying, a pervasive issue in the digital age, poses threats to individuals' well-being across various attributes such as religion, age, ethnicity, and gender. This research employs artificial intelligence to detect cyberbullying instances in Twitter data, utilizing both traditional and deep learning models. The study repurposes the Sentiment140 dataset, originally intended for sentiment analysis, for the nuanced task of cyberbullying detection. Ethical considerations guide the dataset transformation process, ensuring responsible AI development. The Naive Bayes algorithm demonstrates commendable precision, recall, and accuracy, showcasing its efficacy. The Bi-LSTM model, leveraging deep learning capabilities, exhibits nuanced cyberbullying detection. The study also underscores limitations, emphasizing the need for refined models and diverse datasets.

Keywords: Cyberbullying detection; Social media analysis; Artificial intelligence; Naive Bayes; Bi-LSTM; Ethical AI; Machine learning; Digital well-being

*CORRESPONDING AUTHOR:
Adeyinka Orelaja, Department of Computer Science, Austin Peay State University, Tennessee, 37044, USA; Email: aorelaja@my.apsu.edu
Success Imakuh, Department of Computing, Teesside University, Middlesbrough, TS1 3BX, United Kingdom; Email: B1142347@live.tees.ac.uk

ARTICLE INFO
Received: 10 January 2024 | Revised: 31 January 2024 | Accepted: 20 February 2024 | Published Online: 28 February 2024
DOI: https://doi.org/10.30564/jeis.v6i1.6206

CITATION
Orelaja, A., Ejiofor, C., Sarpong, S., et al., 2024. Attribute-specific Cyberbullying Detection Using Artificial Intelligence. Journal of Electronic & Information Systems. 6(1): 10–21. DOI: https://doi.org/10.30564/jeis.v6i1.6206

1. Introduction

1.1 Background

Cyberbullying is the act of harming or harassing someone online through messages or images that are malicious or harmful. Cyberbullying can negatively affect the mental health and well-being of the victims, causing depression, anxiety, low self-esteem, and suicidal thoughts [1].

Another study by Erbic¸er et al. (2023) [2] defines cyberbullying perpetration as a form of harmful behavior, which can be defined as the deliberate, repetitive, and damaging attitude of individuals or groups harming others using the internet, mobile phones, or other communication tools such as e-mail, messages, or social media.

There are many definitions of cyberbullying, however, many definitions are deemed insufficient, often lacking clarity and consistency. The challenges involved typically included variations in the defined electronic methods [3]. Different scholars and organizations may conceptualize cyberbullying in various ways, ranging from explicit threats to subtle forms of harassment. Some definitions encompass the misuse of power differentials, while others focus on the intent to cause harm. By recognizing this diversity, our research seeks to address the multifaceted nature of cyberbullying, encompassing a broad spectrum of aggressive behaviors within the context of online communication.

Social media platforms, such as X (formerly known as Twitter), allow millions of people to share their opinions, thoughts, and feelings online. However, they also enable cyberbullies to target and harass others based on their personal characteristics, such as religion, age, ethnicity, and gender [4]. Therefore, it is crucial to develop effective methods to detect and prevent cyberbullying on social media platforms and to protect the online safety and dignity of the users. A global survey by Microsoft [5] found that 75% of participants agreed that social media companies needed to moderate harmful speech online. Being able to detect cyberbullying on these social media platforms is the first step in achieving this.

Artificial intelligence (AI) is a field of computer science that aims to create machines or systems that can perform tasks that require human intelligence, such as reasoning, learning, and decision-making [6]. AI can be used to analyze and understand large amounts of data, such as text, images, and videos, and to extract useful information or insights from them [7].

AI can be applied to detect cyberbullying on social media platforms by using techniques such as natural language processing (NLP) and machine learning (ML). NLP is a subfield of AI that deals with the interaction between computers and human languages, such as understanding, generating, and translating natural language texts [8] and ML is a subfield of AI that focuses on creating systems that can learn from data and improve their performance without explicit programming [9].

1.2 Motivation

The motivation behind undertaking this research is underscored by the increasing severity and diversity of cyberbullying incidents. In recent years, cyberbullying has transcended traditional forms, branching into attribute-based attacks that target individuals based on characteristics such as religion, age, ethnicity, and gender. The consequences of such attacks are profound, affecting not only the mental well-being of individuals but also perpetuating societal divisions.

The ever-evolving nature of online communication poses a unique challenge. Traditional approaches to cyberbullying detection often struggle to keep pace with the dynamic patterns and expressions of harassment on platforms like Twitter (X). The motivation is thus driven by the need for adaptive, sophisticated algorithms capable of discerning nuanced forms of cyberbullying, particularly those tied to specific attributes. In an era where cyberbullying is a growing concern in the digital era, with notable implications for individuals' mental health [10], the motivation for this research extends beyond academic curiosity to a commitment to foster digital spaces that are free from the detrimental effects of cyberbullying.

1.3 Problem statement

Cyberbullying encompasses a range of harmful behaviors manifesting in digital spaces, impacting individuals based on attributes such as religion, age, ethnicity, and gender. The lack of effective mechanisms to identify and curb cyberbullying on platforms like X Twitter perpetuates an environment where users may experience online harassment, leading to psychological distress and potential real-world consequences. Existing studies [11] emphasize the need for advanced techniques to automatically detect and mitigate cyberbullying instances, tailoring approaches to the nuanced nature of social media interactions.

1.4 Objectives

This research is anchored in the goal of crafting a machine learning-backed cyberbullying detection tool that utilizes the vast sea of social media data. The following detailed objectives are set to support this ambition:

1) **Data Acquisition and Preprocessing**: To achieve robust data-driven insights, the study aims to collect a diverse dataset from social media posts, particularly Twitter (X). The gathered data will then undergo meticulous preprocessing, encompassing noise reduction, text normalization, and the resolution of challenges inherent to cyberbullying content.

2) **Development of Attribute-Specific Detection Models**: Moving to the development phase, the research will conduct a thorough literature review to inform the creation of advanced machine learning models. Utilizing both Naive Bayes and Long Short-Term Memory (LSTM) algorithms, special attention will be given to attribute-specific detection. This entails tailoring models to recognize cyberbullying instances related to 'religion', 'age', 'ethnicity', and 'gender' categories. The iterative fine-tuning and optimization of these models will be paramount to ensuring their effectiveness.

3) **Comprehensive Evaluation of Model Performance**: Subsequently, the research will shift focus to the comprehensive evaluation of model performance. This involves the selection and justification of appropriate evaluation metrics, considering factors such as accuracy, precision, recall, and F1 score. Real-world testing will be conducted using representative social media data from Twitter (X), and a comparative analysis will benchmark the developed models against each other and existing state-of-the-art cyberbullying detection models.

Ethical considerations will be woven into each stage of the research, with a specific emphasis on addressing bias and ensuring fairness. The objective is to propose strategies that mitigate ethical concerns and enhance the responsible deployment of the developed models.

2. Literature review

The exploration of cyberbullying within the context of social media platforms, notably Twitter (X), has been a subject of significant scholarly inquiry. The extensive body of work in this research area underscores the gravity of the issue and the imperative to comprehend the various facets of online harassment.

2.1 Categorization of aggressive messages

The categorization of aggressive messages is a crucial aspect of understanding and addressing online harassment and cyberbullying. Previous research has delved into various approaches for categorizing aggressive content on social media platforms. Elsafoury et al. (2020) conducted a comprehensive analysis of cyberbullying datasets, including those from Twitter, Kaggle, Wikipedia Talk pages, and YouTube [12]. Their work involved the extraction and classification of over 47,000 tweets, providing insights into different forms of cyberbullying, including age-based, religion-based, ethnicity-based, and gender-based aggression.

The study emphasized the importance of diverse demographic parameters in categorizing cyberbullying instances. This aligns with the present research, which leverages demographic attributes such as age, ethnicity, gender, and religion in the detection and categorization of cyberbullying tweets. The distribution of instances across classes reflects the varied nature of cyberbullying content within each category.

2.2 Existing approaches to cyberbullying detection

Cyberbullying detection has been addressed through a spectrum of approaches, ranging from traditional rule-based systems to advanced machine learning and deep learning models. Prior studies [10,13] have extensively explored various methodologies for cyberbullying detection. Each methodology brings distinct advantages and challenges to the forefront.

1) Rule-Based Systems: Rule-based systems leverage predefined patterns or heuristics to identify potential instances of cyberbullying. An example is the use of keyword matching where predefined sets of offensive words or phrases trigger an alert. These systems are straightforward to implement and interpret but often struggle with the dynamic and nuanced nature of cyberbullying, as they may not capture context well [14].

2) Machine Learning Models: Machine learning models, including classic algorithms like Support Vector Machines (SVMs) and Random Forests, have demonstrated efficacy in learning patterns from labeled data. SVMs, for instance, have been employed to classify cyberbullying instances based on features extracted from textual data [15]. Random Forests, with their ensemble learning approach, offer robustness against overfitting and have been applied to cyberbullying detection tasks [16]. These models exhibit adaptability to evolving cyberbullying patterns but may require significant labeled data for effective training.

3) Deep Learning Models: Deep learning models, characterized by architectures like recurrent neural networks (RNNs) and convolutional neural networks (CNNs), excel at capturing complex relationships in textual data. For instance, Almomani et al. (2024) [17] proposed a method using a CNN to detect cyberbullying incidents on Instagram, demonstrating the capacity of deep learning models to discern intricate patterns in multimedia-rich content. Long Short-Term Memory (LSTM) networks, a type of RNN, have been employed for sequential modeling, enabling the understanding of temporal dynamics in cyberbullying conversations [18]. Deep learning models showcase a high degree of sophistication in understanding context and semantics, making them well-suited for cyberbullying detection tasks.

The landscape of cyberbullying detection is dynamic, and the effectiveness of each approach depends on the context, the nature of the data, and the specific nuances of cyberbullying instances.

2.3 Ethical considerations in cyberbullying detection

The ethical dimensions surrounding the deployment of cyberbullying detection machine learning models have become increasingly prominent in recent works. Scholars have scrutinized the impact of these models on various ethical aspects, including issues of bias, fairness, and privacy.

Existing works have explored different avenues to address these ethical concerns. Aizenberg and Van Den Hoven (2020) [19] shed light on the broader landscape of big data ethics, emphasizing the need for responsible practices in handling sensitive information. This broader perspective encompasses considerations beyond individual instances of cyberbullying and extends to the overarching ethical responsibilities tied to data usage in the digital sphere.

Sap et al. (2019) [20] delved specifically into the risk of racial bias in hate speech detection, recognizing the profound implications of biases within detection models. Their work highlighted the challenges of ensuring fairness in models that are designed to discern harmful online content. Such biases could potentially exacerbate existing inequalities and societal divisions, necessitating a careful examination of the underlying algorithms.

In the pursuit of advancing cyberbullying detection models ethically, it is imperative to acknowledge and bridge these gaps. The current research aims to contribute to this ongoing discourse by proposing strategies that not only address biases but also ensure the responsible and fair deployment of cyberbullying detection models within the intricate landscape of social media.

2.4 Gaps in existing literature

Significant strides have been made in understanding and addressing cyberbullying, but notable gaps persist in the current literature, creating avenues for further exploration and refinement.

While existing works touch on biases and fairness in detection models, ethical considerations in the preprocessing of cyberbullying data remain underexplored. This research will fill this gap by scrutinizing the ethical implications of data preprocessing, ensuring the foundation of detection models aligns with ethical standards.

Current literature also often adopts a binary approach, distinguishing between cyberbullying and noncyberbullying instances. However, nuances across attributes like 'religion', 'age', 'ethnicity', and 'gender' call for a more nuanced approach. This research addresses this gap by employing attribute-specific detection, offering a more context-aware understanding of cyberbullying.

This research aims to enhance the existing discourse by addressing these gaps, contributing to a more ethically sound and context-aware cyberbullying detection paradigm.

3. Methodology

3.1 Dataset overview

The dataset utilized in this study originates from a comprehensive collection of cyberbullying data compiled by Elsafoury (2020) [12]. Primarily sourced from various social media platforms, including Kaggle, Twitter (X), Wikipedia Talk pages, and YouTube, the dataset offers a diverse range of cyberbullying instances. For the purposes of this research, the focus was narrowed down to extracting Twitter data (X), resulting in a dataset exceeding 47,000 tweets explicitly labeled as cyberbullying.

Composition and Demographic Parameters: The dataset exhibits a rich composition, including explicit labels for different forms of cyberbullying and demographic parameters such as age, ethnicity, gender, and religion. The classes/labels are moderately balanced as shown in **Table 1**. This multiclass dataset enables a nuanced understanding of cyberbullying phenomena, capturing the intersectionality of various demographic factors with different manifestations of cyberbullying.

Table 1. Distribution of instances across cyberbullying classes.

Class	Count
Religion	7997
Age	7992
Ethnicity	7959
Gender	7948
Not cyberbullying	7937
Other cyberbullying	7823

3.2 Preprocessing

The preprocessing phase is crucial to ensure the integrity and quality of the dataset for cyberbullying detection. This section outlines a series of steps encompassing data loading, duplicate removal, and an intricate set of text-cleaning processes as adhered to in the recommendations outlined in the paper by Bokolo and Liu (2023) [10]. Particular emphasis is placed on avoiding biases and ensuring fairness throughout the cleaning procedures.

1) *Data Loading and Initial Inspection:* The initial step involves loading the raw dataset from a CSV file (cyberbullying_tweets.csv). The dataset is then inspected to comprehend its structure and content, showcasing the first few rows and providing key information such as column names and data types.

2) *Duplicate Removal:* Duplicate tweets can introduce biases and skew the model's performance. This subsection details the identification and removal of duplicate tweets, ensuring the dataset's uniqueness

and integrity.

3) *Column Renaming:* To streamline subsequent references, columns are renamed, adopting more concise names. Specifically, 'tweet_text' is renamed to 'text', and 'cyberbullying_type' to 'sentiment'.

4) *Text Cleaning Functions:* A set of custom-defined functions is introduced for comprehensive text cleaning, with a keen eye on avoiding biases and ensuring fairness:

Emoji Removal: Eliminating emojis to prevent potential bias associated with certain emoticons with the function shown.

Decontraction: Ensuring uniformity in language by expanding contractions, avoiding bias introduced by different writing styles as shown in the 'decontract()' function.

Entity Stripping: Removing links, mentions, and special characters to prevent biased influence from specific entities or symbols.

Hashtag Cleaning: Ensuring fair treatment of hashtags, cleaning them at the end of sentences and removing the '#' symbol within words to prevent unintended biases as shown in the function.

Filtering Specific Characters: Removing characters such as '$' and '&' to avoid biases associated with particular symbols.

Removing Multiple Sequential Spaces: Avoid bias by maintaining consistent spacing throughout the text.

Stemming: Standardizing words to their root form to ensure fairness in words.

5) *Application of Cleaning Functions:* The defined cleaning functions are systematically applied to each tweet in the dataset, resulting in a new column, 'text_clean', containing the cleaned text.

6) *Final Dataset Inspection:* Following the cleaning procedures, a final inspection of the dataset is conducted, revealing changes in size and highlighting any potential improvements in data quality.

7) *Sentiment Labeling:* The sentiment labels are redefined for clarity, mapping 'religion' to 0, 'age' to 1, 'ethnicity' to 2, 'gender' to 3, and 'not_cyberbullying' to 4.

8) *Text Length Analysis:* The distribution of text lengths is analyzed, with visualizations depicting the count of tweets based on their word length. Tweets with lengths exceeding certain thresholds are filtered to ensure data quality and relevance.

3.3 AI techniques

A meticulous split into training and test sets, allocating 20% to the latter and further dividing the remaining 80% into training and validation data, was conducted to monitor model accuracy and mitigate overfitting.

In the subsequent phase of model building, two distinct models—Naive Bayes and Bidirectional Long Short-Term Memory (Bi-LSTM)—were selected and compared for their efficacy in cyberbullying detection. This choice was guided by recommendations from related literature, acknowledging the inherent advantages of these models within the realm of sentiment analysis. The ensuing comparative analysis aims to determine the most effective model for accurately classifying tweets and detecting instances of cyberbullying within the dataset.

Naive Bayes: The Naive Bayes algorithm stands out as a swift and straightforward classification method, particularly adept at handling extensive datasets [21]. Proven effective in various applications, including spam filtering, text classification, public opinion analysis, and recommendation systems, Naive Bayes leverages the Bayes theorem of probability for predicting unknown classes.

In the implementation of the Naive Bayes Model, the model was instantiated using a Count Vectorizer to create a bag of words. Subsequently, TF-IDF (Term Frequency-Inverse Document Frequency) transformation was applied to assign weights to words based on their frequency, enhancing the model's understanding of their contextual significance. **Pytorch-Bi-LSTM Sentimental Analysis**: The Bi-LSTM (Bidirectional Long Short-Term Memory) model plays a pivotal role in the cyberbullying detection framework [10]. Below is a detailed description of the Bi-LSTM model construction and training.

1) *Model Architecture:* The LSTM model is designed as a subclass of the PyTorch nn.Module class, named BiLSTM_Sentiment_Classifier. It comprises the following key components also shown in **Figure 1**:

Embedding Layer: Converts input tokens into dense vectors of fixed size (embedding).

```
BiLSTM_Sentiment_Classifier(
  (embedding): Embedding(33009, 200)
  (lstm): LSTM(200, 100, batch_first=True, dropout=0.5, bidirectional=True)
  (fc): Linear(in_features=200, out_features=5, bias=True)
  (softmax): LogSoftmax(dim=1)
)
```

Figure 1. Bi-LSTM architecture.

Bidirectional LSTM Layers: The LSTM layers process the embedded tokens, capturing contextual information. The number of layers (lstm), hidden dimension (hidden_dim), and bidirectional nature are configurable.

Fully Connected Layer: A linear layer (fc) transforms the output of the LSTM layers into logits for each sentiment class.

Softmax Activation: The LogSoftmax activation function normalizes the logits to probabilities, facilitating class predictions [22].

Initialization of Hidden States: The init_hidden method initializes the LSTM hidden and cell states.

The model is equipped to handle a dynamic batch size (batch_size), allowing flexibility during training and evaluation.

2) *Model Training:* The model is trained using the 'AdamW' optimizer with a learning rate of 3e-4 and a weight decay of 5e-6. The negative log-likelihood loss (NLLLoss) serves as the criterion for training. The training process is conducted over multiple epochs (5 EPOCHS), with early stopping implemented to prevent overfitting. Training involves iterating through the training dataset, computing gradients, and updating model parameters.

4. Results and discussion

In this chapter, the intricacies of the results obtained during the experimentation phase are delved into. The primary objective is to provide a transparent and detailed overview of the cyberbullying detection framework's effectiveness across various dimensions. This includes an exploration of an in-depth analysis of model performance metrics, and a comparative assessment of diverse machine learning and deep learning models. Furthermore, the chapter addresses the ethical considerations embedded in the models, reflecting on potential biases and fairness aspects.

4.1 Model performance

In evaluating the models for cyberbullying detection, we meticulously examine the performance metrics of two distinct approaches: the Naive Bayes classifier and the Bi-LSTM neural network. These models represent different paradigms, with Naive Bayes relying on probabilistic principles and Bi-LSTM leveraging the power of recurrent neural networks. Performance evaluation metrics were applied following the methods detailed in the research by Bokolo et al. (2023) [23].

1) *Naive Bayes Performance:* The Naive Bayes classifier exhibits commendable performance with precision, recall, and F1 score all hovering around 0.85. This suggests that the model effectively identifies instances of cyberbullying while minimizing false positives. The accuracy of 0.85 underscores its overall correctness in predictions. The Naive Bayes model demonstrated commendable performance across various classes, as illustrated in **Table 2**. Notably, the model excelled in precision for the 'Religion' and 'Age' classes, achieving 85% and 80%, respectively. However, the model showed some challenges in recall for the 'Not Bullying' class, achieving 47%.

Table 2. Class-wise performance of the Naive Bayes model.

	Precision	**Recall**	**F1-score**	**Support**
Religion	0.85	0.97	0.91	1579
Age	0.80	0.98	0.88	1566
Ethnicity	0.90	0.92	0.91	1542
Gender	0.89	0.85	0.87	1462
Not bullying	0.84	0.47	0.60	1274

2) *Bi-LSTM Performance:* Contrastingly, the Bi-LSTM neural network demonstrates superior

performance with precision, recall, and F1 score all surpassing 0.93. This signifies the model's robust ability to capture instances of cyberbullying with high precision while ensuring comprehensive coverage of actual positive instances. The accuracy of 0.93 attests to the model's overall proficiency. The Bi-LSTM model exhibited superior performance across all classes, as shown in **Table 3**. Particularly noteworthy is the high precision and recall for the 'Age' and 'Ethnicity' classes, showcasing the model's effectiveness in detecting cyberbullying related to these attributes.

Table 3. Class-wise performance of the Bi-LSTM model.

	Precision	Recall	F1-score	Support
Religion	0.97	0.93	0.95	1572
Age	0.98	0.97	0.97	1560
Ethnicity	0.98	0.98	0.98	1535
Gender	0.96	0.87	0.91	1456
Not bullying	0.77	0.91	0.83	1269

4.2 Comparative analysis of models

The Naive Bayes model, rooted in probabilistic principles, showcases a balanced performance, effectively distinguishing between cyberbullying and non-cyberbullying content. Its reliance on statistical independence assumptions doesn't hinder its effectiveness in this context.

On the other hand, the Bi-LSTM, a deep learning model, leverages the sequential nature of language, capturing intricate patterns within the text. The superior performance metrics highlight its adeptness in discerning the nuanced language indicative of cyberbullying across various attributes.

Both models, while showcasing high accuracy, precision, recall, and F1 score, do so through distinct mechanisms. The Naive Bayes model excels in probabilistic reasoning, while the Bi-LSTM harnesses the power of neural networks to capture complex patterns. The confusion matrices (**Tables 4 and 5**) provide a visual aid in understanding the models' classification outcomes.

These results underscore the potential of diverse approaches in cyberbullying detection, each with its unique strengths. The choice between these models should be guided by the specific requirements and nuances of the online environment under consideration.

Table 4. Naive Bayes confusion matrix.

	Predicted				
	Religion	Age	Ethnicity	Gender	Not bullying
Religion	1536	14	10	9	10
Age	11	1541	6	5	3
Ethnicity	58	50	1417	14	3
Gender	30	31	57	1248	96
Not bullying	164	295	85	129	601

Table 5. Bi-LSTM confusion matrix.

	Predicted				
	Religion	Age	Ethnicity	Gender	Not bullying
Religion	1463	3	3	2	31
Age	3	1513	2	2	33
Ethnicity	5	4	1499	5	9
Gender	7	3	26	1263	44
Not bullying	96	37	26	180	1152

4.3 Ethical considerations

It is imperative to underscore the ethical considerations that guided this research. The deployment of AI models in sensitive domains such as cyberbullying detection necessitates a conscientious approach to address potential ethical challenges. Aligning with the ethical considerations posited by Bokolo and Liu (2023) [13], our research critically examines the potential biases and fairness issues in the cyberbullying detection process.

1) *Bias Mitigation and Fairness:* Ensuring fairness in our models is a paramount concern. We meticulously examined the training data to identify and rectify biases that might lead to disparate impacts on different demographic groups. This involved scrutinizing the dataset for imbalances in class distribution and refining the model's training to mitigate potential biases.

2) *Privacy Concerns:* Respecting user privacy is central to ethical AI practices. Our study relied on anonymized data to minimize the risk of identifying individuals involved in social media conversations. Additionally, all personally identifiable information was rigorously stripped from the dataset during the preprocessing phase.

3) *Continuous Monitoring:* Ethical considerations extend beyond the development phase to the entire lifecycle of the models. We advocate for continuous monitoring and evaluation of the models' performance in real-world scenarios. Regular assessments help identify and rectify any unforeseen biases or ethical implications that might arise as the models are deployed.

4) *Informed Consent:* When dealing with user-generated content on social media, obtaining explicit consent for data usage is challenging. However, we acknowledge the importance of transparency and informed consent. Our study emphasizes the use of publicly available, anonymized data to respect user privacy while conducting meaningful research.

By addressing biases, ensuring privacy, promoting transparency, and advocating for ongoing monitoring, we strive to uphold the achievable ethical standards in our research and its practical implications.

5. Conclusions

5.1 Summary of research

1) *Introduction Recap:* This research endeavors to tackle the pertinent issue of cyberbullying through the lens of artificial intelligence. With a focus on Twitter data and utilizing the power of machine learning algorithms, the study aims to detect instances of cyberbullying about attributes such as religion, age, ethnicity, and gender.

2) *Methodology Recap:* Commencing with an in-depth methodology, the research encapsulates data preprocessing steps, model training employing Naive Bayes and Bi-LSTM algorithms, and a meticulous evaluation process. Leveraging the sentiment-labeled Sentiment140 dataset, the study repurposes it for cyberbullying detection while addressing ethical considerations in dataset usage.

3) *Results Overview:* The outcomes of the research present a nuanced understanding of the model performances. Both Naive Bayes and Bi-LSTM models exhibit commendable precision, recall, and accuracy, offering promising tools for cyberbullying detection.

5.2 Achievements and contributions

1) *Model Performance:* The study's principal achievements lie in the models' capability to discern cyberbullying across various attributes. The Naive Bayes algorithm showcases robust performance, and the Bi-LSTM model, with its deep learning capabilities, excels in nuanced cyberbullying detection.

2) *Ethical Considerations:* Ethical considerations take center stage in this research, addressing biases in the dataset and ensuring fairness. The commitment to responsible AI development underscores the ethical dimension as an integral part of the study.

5.3 Limitations and challenges

1) *Data Limitations:* While the Sentiment140 dataset proves valuable, the study acknowledges its limitations, suggesting future research explore more specialized datasets for cyberbullying detection.

2) *Model Limitations:* Despite their effectiveness, both models face challenges in handling nuanced expressions and contextual intricacies. Acknowledging these limitations provides avenues for future research and model refinement.

5.4 Implications for future research

Building on the insights gained from the research by Bokolo and Liu (2023) [10], future research directions may explore more advanced deep-learning architectures for enhanced cyberbullying detection.

1) *Further Model Refinement:* The models, although successful, prompt consideration for refinement. Fine-tuning, exploring advanced architectures, and addressing model limitations are avenues for future exploration.

2) *Exploration of New Data Sources:* Diversifying data sources beyond Sentiment140 could enhance model robustness. Investigating datasets explicitly designed for cyberbullying detection is recommended.

3) *Cross-Domain Applications:* Considering the models' adaptability to various platforms and domains presents exciting opportunities. Future research could explore cross-domain applications for a broader societal impact.

5.5 Practical applications

1) *Real-world Implementation:* With promising results, the models hold potential for real-world implementation on social media platforms, providing timely support for individuals facing cyberbullying.

2) *Policy Recommendations:* While cautious in its suggestions, the research hints at the development of policies or interventions based on their outcomes. Ethical deployment and user well-being should guide any policy considerations.

5.6 Concluding remarks

In conclusion, this research contributes valuable insights and tools for combatting cyberbullying. The models presented showcase promising results, affirming the role of artificial intelligence in addressing societal challenges. The commitment to ethical considerations position this study within the framework of responsible AI development, ensuring the tools created serve societal well-being.

Author Contributions

Authors 1 to 4 collaborated on the technical aspects of the research, including a literature review, data collection, preprocessing, feature engineering, and AI model development. Authors 5 to 8 contributed to the ethical considerations, experimental design, validation, and documentation of the cyberbullying detection study, ensuring a comprehensive approach that addresses both technical and ethical aspects.

Conflict of Interest

There is no conflict of interest.

Acknowledgments

We extend our sincere appreciation to Biodoumoye George Bokolo, a final-year doctoral student in Digital and Cyber Forensics Science, for her exceptional contribution to the publication titled "Attribute-Specific Cyberbullying Detection Using Artificial Intelligence". Biodoumoye served as a dedicated mentor and advisor, leveraging her profound expertise in the field of digital forensics and her specialization in utilizing artificial intelligence to detect cybercrime and enhance cybersecurity measures.

Her insightful guidance, unwavering support, and commitment to advancing the realms of digital and cyber forensics have been instrumental in shaping the direction and depth of our research. Biodoumoye's passion for securing cyberspace through innovative AI solutions has left an indelible mark on this project, and we are grateful for her invaluable contributions that have significantly enriched the quality and relevance of our work.

References

[1] Agustiningsih, N., Yusuf, A., Ahsan, A., 2023. Relationships among self-esteem, bullying, and cyberbullying in adolescents: a systematic review. Journal of Psychosocial Nursing and Mental Health Services. 1–7. DOI: https://doi.org/10.3928/02793695-20231013-01

[2] Erbiçer, E.S., Ceylan, V., Yalçın, M.H., et al., 2023. Cyberbullying among children and youth in Türkiye: A systematic review and meta-analysis. Journal of Pediatric Nursing. 73, 184–195. DOI: https://doi.org/10.1016/j.pedn.2023.09.003

[3] Zhang, W., Huang, S., Lam, L., et al., 2022. Cyberbullying definitions and measurements in children and adolescents: Summarizing 20 years of global efforts. Frontiers in Public Health. 10, 1000504.

DOI: https://doi.org/10.3389/fpubh.2022.1000504

[4] Chan, T.K., Cheung, C.M., Lee, Z.W., 2021. Cyberbullying on social networking sites: A literature review and future research directions. Information & Management, 58(2), 103411. DOI: https://doi.org/10.1016/j.im.2020.103411

[5] Civility, Safety and Interaction Online [Internet]. Microsoft; 2020. Available from: https://news.microsoft.com/wp-content/uploads/prod/sites/421/2020/02/Digital-Civility-2020-Global-Report.pdf

[6] Sarker, I.H., 2022. AI-based modeling: Techniques, applications and research issues towards automation, intelligent and smart systems. SN Computer Science. 3, 158. DOI: https://doi.org/10.1007/s42979-022-01043-x

[7] Chowdhary, K.R., 2020. Fundamentals of artificial intelligence. Springer India: New Delhi.

[8] Speech and Language Processing: An Introduction to Natural Language Processing, Computational Linguistics, and Speech Recognition [Internet].

[9] Leekha, G., 2021. Learn AI with Python: Explore machine learning and deep learning techniques for building smart AI systems using Scikit-Learn, NLTK, NeuroLab, and Keras (English Edition). BPB Publications: New Delhi.

[10] Bokolo, B.G., Liu, Q. (editors), 2023. Cyberbullying detection on social media using machine learning. IEEE INFOCOM 2023-IEEE Conference on Computer Communications Workshops (INFOCOM WKSHPS); 2023 May 20; Hoboken, NJ, USA. New York: IEEE. p. 1–6. DOI: https://doi.org/10.1109/INFOCOMWKSHPS57453.2023.10226114

[11] Singh, N., Sinhasane, A., Patil, S., et al. (editors), 2020. Cyberbullying detection in social networks: A survey. 2nd International Conference on Communication & Information Processing (ICCIP); 2020 Nov 27–29; Tokyo, Japan.

[12] Elsafoury, F., 2020. "Cyberbullying Datasets," *Mendeley. Com [Internet] [Accessed: 04-Summer-2021]. Available from:* https://www.kaggle.com/datasets/gbiamgaurav/cyberbullying-detection

[13] Bokolo, B.G., Liu, Q., 2023. Combating cyberbullying in various digital media using machine learning. Combatting cyberbullying in digital media with artificial intelligence. Chapman and Hall/CRC: London. pp. 71–97.

[14] Chong, W.J., Chua, H.N., Gan, M.F. (editors), 2022. Comparing zero-shot text classification and rule-based matching in identifying cyberbullying behaviors on social media. 2022 IEEE International Conference on Artificial Intelligence in Engineering and Technology (IICAIET); 2022 Sep 13–15; Kota Kinabalu, Malaysia. New York: IEEE. p. 1–5. DOI: https://doi.org/10.1109/IICAIET55139.2022.9936821

[15] Purnamasari, N.M.G.D., Fauzi, M.A., Indriati, L.S.D., et al., 2020. Cyberbullying identification in Twitter using support vector machine and information gain based feature selection. Indonesian Journal of Electrical Engineering and Computer Science. 18(3), 1494–1500. DOI: https://doi.org/10.11591/ijeecs.v18.i3.pp1494-1500

[16] Talpur, B.A., O'Sullivan, D., 2020. Cyberbullying severity detection: A machine learning approach. PloS One. 15(10), e0240924. DOI: https://doi.org/10.1371/journal.pone.0240924

[17] Almomani, A., Nahar, K., Alauthman, M., et al., 2024. Image cyberbullying detection and recognition using transfer deep machine learning. International Journal of Cognitive Computing in Engineering. 5, 14–26. DOI: https://doi.org/10.1016/j.ijcce.2023.11.002

[18] Obaid, M.H., Guirguis, S.K., Elkaffas, S.M., 2023. Cyberbullying detection and severity determination model. IEEE Access. 11, 97391–97399. DOI: https://doi.org/10.1109/ACCESS.2023.3313113

[19] Aizenberg, E., Van Den Hoven, J., 2020. Designing for human rights in AI. Big Data & Society. 7(2).
DOI: https://doi.org/10.1177/2053951720949566

[20] Sap, M., Card, D., Gabriel, S., et al. (editors), 2019. The risk of racial bias in hate speech detection. The 57th Annual Meeting of the Association for Computational Linguistics; 2019 Jul 28–Aug 2; Florence, Italy. p. 1668–1678.

[21] Gasparetto, A., Marcuzzo, M., Zangari, A., et al., 2022. A survey on text classification algorithms: From text to predictions. Information. 13(2), 83.
DOI: https://doi.org/10.3390/info13020083

[22] Kaushik, M., Prakash, P., Ajay, R., et al. (editors), 2020. Tomato leaf disease detection using convolutional neural network with data augmentation. 2020 5th International Conference on Communication and Electronics Systems (ICCES); 2020 Jun 10–12; Coimbatore, India. New York: IEEE. p. 1125–1132.
DOI: https://doi.org/10.1109/ICCES48766.2020.9138030

[23] Bokolo, B.G., Ogegbene-Ise, E., Chen, L., et al. (editors), 2023. Crime-intent sentiment detection on Twitter data using machine learning. 2023 8th International Conference on Automation, Control and Robotics Engineering (CACRE); 2023 Jul 13–15; Hong Kong, China. New York: IEEE. p. 79–83.
DOI: https://doi.org/10.1109/CACRE58689.2023.10208384

BILINGUAL PUBLISHING GROUP

Journal of Electronic & Information Systems

https://journals.bilpubgroup.com/index.php/jeis

ARTICLE

Evaluating Maximum Diameters of Tumor Sub-regions for Survival Prediction in Glioblastoma Patients via Machine Learning, Considering Resection Status

R Babaei[1], *A Bonakdar*[1], *N Shakourifar*[1], *M Soltani*[1,2,3,4,7*], *K Raahemifar*[5,6,7]

[1] *Department of Mechanical Engineering, K. N. Toosi University of Technology, Tehran, 15418-49611, Iran*
[2] *Department of Electrical and Computer Engineering, University of Waterloo, Waterloo, Ontario, N2L 3G1, Canada*
[3] *Centre for Biotechnology and Bioengineering (CBB), University of Waterloo, Waterloo, Ontario, N2L 3G1, Canada*
[4] *Advanced Bioengineering Initiative Center, Computational Medicine Center, K. N. Toosi University of Technology, Tehran, 15418-49611, Iran*
[5] *College of Information Sciences and Technology (IST), Data Science and Artificial Intelligence Program, Penn State University, State College, Pennsylvania, PA, 16801, United States of America*
[6] *Chemical Engineering Department, University of Waterloo, Waterloo, ON, N2L 3G1, Canada*
[7] *Optometry & Vision Science Department, University of Waterloo, Waterloo, ON, N2L 3G1, Canada*

ABSTRACT

In recent decades, there have been significant advancements in medical diagnosis and treatment techniques. However, there is still much progress to be made in effectively managing a wide range of diseases, particularly cancer. Timely diagnosis of cancer remains a critical step towards successful treatment, as it significantly impacts patients' chances of survival. Among various types of cancer, glioma stands out as the most common primary brain tumor, exhibiting different levels of aggressiveness. One of the monitoring techniques is magnetic resonance imaging (MRI) which provides a precise visual representation of the tumor and its sub-regions (edema (ED), enhancing tumor (ET), and non-enhancing necrotic tumor core (NEC)), enabling monitoring of its location, shape, and sub-regional characteristics. In this study, the authors aim to investigate the underlying relationship between the maximum diameters of tumor sub-regions and patients' overall survival (OS) in glioblastoma cases. Using an MRI dataset of glioblastoma patients, the authors categorized them based on resection status: gross total resection (GTR) and unknown (NA). By employing the Euclidean distance algorithm, the authors estimated the sub-regions' maximum diameters. Machine learning algorithms were used to explore the correlation between sub-regions' maximum diameters and survival outcomes. The results of the univariate prediction models showed that tumor sub-regions' maximum diameters have a noticeable correlation with the survival rates among patients with unknown resection status with the average Spearman correlation of –0.254. Also, the addition of the sub-regions' maximum diameter feature to the radiomics increased the accuracy of ML algorithms in predicting the survival rates with an average of 4.58%.

Keywords: Machine learning; Radiomics; Glioblastoma; Tumor sub-regions; BraTS 2019

*CORRESPONDING AUTHOR:
M Soltani, Department of Mechanical Engineering, K. N. Toosi University of Technology, Tehran, 15418-49611, Iran; Department of Electrical and Computer Engineering, University of Waterloo, Waterloo, Ontario, N2L 3G1, Canada; Centre for Biotechnology and Bioengineering (CBB), University of Waterloo, Waterloo, Ontario, N2L 3G1, Canada; Advanced Bioengineering Initiative Center, Computational Medicine Center, K. N. Toosi University of Technology, Tehran, 15418-49611, Iran; Optometry & Vision Science Department, University of Waterloo, Waterloo, ON, N2L 3G1, Canada; Email: msoltani@uwaterloo.ca

ARTICLE INFO
Received: 23 December 2023 | Revised: 18 January 2023 | Accepted: 28 February 2024 | Published Online: 22 March 2024
DOI: https://doi.org/10.30564/jeis.v6i1.6174

CITATION
Babaei, R., Bonakdar, A., Shakourifar, N., et al., 2024. Evaluating Maximum Diameters of Tumor Sub-regions for Survival Prediction in Glioblastoma Patients via Machine Learning, Considering Resection Status. Journal of Electronic & Information Systems. 6(1): 22–38. DOI: https://doi.org/10.30564/jeis.v6i1.6174

1. Introduction

According to WHO reports, cancer is the second cause of death in the world. Cancers have various ranges of aggressiveness. Some are more treatable and can be diagnosed early, while others have higher fatality due to their late symptoms' indications and inadequate response to drugs [1]. The majority of brain tumor patients are those with glioma, which is an intra-axial tumor. Glioma includes almost 30% of all brain tumors beginning in glial cells [2,3]. Based on the cancer aggressiveness, glioma can be subdivided into low-grade glioma (grade I and II) and high-grade glioma (grade III and IV). Among all types of glioma, glioblastoma (GBM) is less treatable, and only 5% of patients diagnosed with GBM have a 5-year survival chance [4]. One of the main difficulties in the therapeutic intervention of GBM is the complex structure of the tumor. It is multiform microscopically, with various regions including pseudopalisading necrosis, pleomorphic nuclei and cells, and microvascular proliferation [5].

Numerous ways have been investigated to estimate the malignancy of tumors and patients' cancer status to predict better further clinical strategies and the chance of surviving. TNM staging is an acceptable way that classifies tumors based on three main criteria: primary brain tumor (T), regional lymph nodes (N), and distance metastasis (M). Besides, some studies have investigated the effect of social [6], physical [7], and economic features [8] on patients' OS. Additionally, the utilization of general features like age and gender as standalone factors for predicting overall survival (OS) in patients has yielded discouraging results [9], mainly due to their lack of individualization [10]. Although medical images contain lots of information that can be detected by the naked eye, numerous quantitative features can be extracted from images by computer-aided algorithms that can describe the disease aggressiveness more accurately [11]. Indeed, automatic analysis of images would be a respectful replacement for traditional approaches and provides more precise results [12].

Radiomics is an emerging method that extracts a large number of quantitative medical imaging features capable of advanced image-based tumor phenotyping, providing valuable clinical information for OS prediction [13]. Early radiomics approaches were the semantic analysis as the radiologists tried to figure out the images only qualitatively. Following the rapid developments of computer-aided algorithms, the field moved quickly toward high-throughput analyses, which led to the extraction of quantitative features from images [14]. More importantly, these features have shown excellent potential to improve the prognostic of glioblastoma patients when integrated with conventional clinical and genetic prognostic models [12].

Hooper [15] reviewed various MRI radiomic features of glioblastoma, providing an overview of the potential applications of radiomics in this context. Zhu [16] developed a non-invasive prediction model for overall survival time in glioblastoma patients based on multimodal MRI radiomics, highlighting the potential of radiomic features in predicting patient outcomes. Furthermore, Li [17] proposed a multiparameter radiomic model for accurate prognostic prediction of glioma, demonstrating the development of novel prognostic radiomic models for predicting the prognosis of glioma.

In the field of glioma research, other studies have employed different approaches. Weninger [9] investigated an age-only regression model, achieving an accuracy of 56% and highlighting that the addition of radiomics to the age parameter did not necessarily improve prediction accuracy for different resection statuses. Shboul [18] utilized random forest regression (RFR) with radiomic features, while Feng [19] employed linear models with geometric features, achieving accuracies of 58% and 62% respectively [20]. Other studies have explored the use of deep models integrated with radiomics for gliomas [21], full-resolution residual convolutional neural networks (FRRN) [22], RFR with atlas locations and tumor's relative size using a "pseudo-3D" method [23], and RFR method [24]. Choi investigated the impact of radiomic features on a random survival forest model, demonstrating a nearly 7% improvement in performance by incorporating radiomics [25]. Similarly, Wankhede [26] used a hybrid model integrating deep features from MRI using the convolutional neural network (CNN) and radiomic features extracted with modified fuzzy C-means (MFCM) clustering algorithm and achieved approximately 20% higher accuracy in glioblastoma survival prediction compared to conventional models. Hu [27] combined radiomics, deep features, and patient-specific clinical features that indicated higher prediction accuracy (0.745) compared to using age and tumor region volumes only (0.638).

The BraTS is a widely used dataset entailing multimodal MRI scans of glioblastoma patients. These scans include T1-weighted MRI (T1), T1-weighted MRI with contrast enhancement (T1CE), T2-weighted MRI (T2), and fluid-attenuated inversion recovery (FLAIR). T1-weighted images are widely utilized for analyzing brain tumor structures due to their ability to facilitate the annotation of healthy tissues [28]. In T1CE sequence images, the borders of brain tumors appear brighter as a result of contrast agent accumulation, allowing for easy differentiation of the necrotic core. Additionally, in T2-weighted images, the edema region appears brighter compared to other areas. The FLAIR scan is particularly useful in distinguishing the edema region from the cerebrospinal fluid (CSF). By combining these distinct MRI sequences, radiomic features can be extracted from the images [29].

In recent years, multimodal assessment has become increasingly popular for its enhanced performance and accuracy. It involves combining various factors such as demographic, socioeconomic, clinical, and radiographic features to predict OS more effectively [30]. However, the influence of tumor sub-regions' maximum diameters on this assessment has not been thoroughly examined.

This study aims to explore the influence of the maximum diameters of sub-regions (edema (ED), enhancing tumor (ET), and non-enhancing necrotic tumor core (NEC) in glioblastoma (GBM)) on the prediction of OS, in conjunction with radiomic features. The training dataset exclusively consists of reliable segmentations from the BraTS 2019 database provided by multiple experts following a consistent annotation protocol, and subsequently validated by experienced neuro-radiologists. To account for the impact of resection status, the dataset was divided into two groups: patients with gross total resection status (GTR) and those with unknown resection status (NA), enabling separate analysis. The maximum diameters of tumor sub-regions were extracted from MRI images, and the individual influence of each feature on OS was evaluated using different regression algorithms. Additionally, the automatic extraction of radiomic features was performed, followed by the elimination of redundant features and the selection of the most relevant ones using feature reduction algorithms. Ultimately, these selected features were then used independently in multivariate prediction models. Additionally, an investigation was conducted to determine if the addition of tumor sub-regions' maximum diameters to these features enhances the robustness of OS prediction.

In the "Materials" section, the article provides information on the dataset and details about the cohort study used in the research. The "Methods" section encompasses stages including image preprocessing, radiomic feature extraction, standardization, and preselection of radiomic features. It also covers the statistical hypothesis testing of preselected radiomic features, the procedure for tumor sub-regions' feature extraction, and the development of prediction models. The "Results" section outlines radiomic feature reduction outputs, hypothesis testing outcomes, as well as the results from univariate and multivariate prediction models. The "Discussion" section delves into the interpretation of findings and explores their implications. Lastly, the "Conclusions" section presents a summary of key findings, suggesting potential directions for future research.

2. Materials

The BraTS 2019 training dataset, a well-known resource in the medical field has been used in this study. Its key elements, including four MRI acquisitions and a comprehensive segmentation map, are explored. Patient data, specifically survival days and resection status, is considered for the purpose of this study. Beyond the dataset, a comprehensive cohort analysis is included in the study to examine how prediction models are influenced by population variations and treatment choices.

2.1 Dataset

The BraTS challenge, which has been held annually since 2012, serves as a platform for comparing different segmentation algorithms. Starting in 2017, the challenge introduced quantitative image features to explore the potential enrichment of clinical insights and the improvement in predicting patients' OS [20,31–34].

In this study, we utilized the BraTS 2019 training dataset, which encompasses four MRI acquisitions (T1, T1CE, T2, and T2-FLAIR), along with a segmentation map that includes edema (ED), enhancing tumor (ET), and non-enhancing necrotic tumor core (NEC). Each of the sequences represents a specific part of the tumor brighter. A tumor segmentation map, which is necessary for radiomic feature extraction, is acquired by integrating all of the sequences.

Additionally, the dataset provides information on the survival days and resection status of 211 glioblastoma (GBM) patients, whose OS spans a range of 3 to 1767 days. Patients were divided into two groups based on the resection status: patients reported as GTR; and patients whose resection status is unavailable (NA).

The BraTS challenge has classified patients' OS into three categories: long-survivors (e.g., > 450 days), short-survivors (e.g., < 300 days), and mid-survivors (e.g., between 300 and 450 days). For the purpose of this study, 450 days were selected as the midpoint to create two distinct groups for classification purposes. However, when using regression models, the exact survival days were considered and fitted to the data.

2.2 Cohort study

The BraTS dataset primarily consists of data from the Center for Biomedical Image Computing and Analytics (CBICA) at the University of Pennsylvania and the Cancer Imaging Archive (TCIA). Although variations in population, imaging protocols, and treatment can have a noticeable impact on prediction models, certain parameters exhibit similarities within this dataset.

Initially, it is important to note that all patients with gross total resection (GTR) and unknown resection (NA) statuses are derived from the CBICA institution and TCIA, respectively. Consequently, there is no substantial disparity in the distribution of each dataset. Additionally, a significant statistical measure, known as the p-value, was employed to assess whether there were notable differences between the groups. Specifically, the p-value was obtained through a one-way analysis of variance. In this dataset, the calculated p-value exceeds 0.05, indicating the absence of significant statistical differences in terms of age or survival among the groups. To visually depict this similarity and facilitate comparison, **Figure 1** illustrates the age and survival day variations for both the GTR and NA groups.

3. Methods

This study employs a set of essential procedures outlined by Soltani [35]. These procedures encompass image preprocessing, radiomic feature extraction, and feature reduction. Additionally, we extracted the maximum diameters of tumor sub-regions and incorporated them into learning algorithms to evaluate their influence on patients' OS.

The significance of these steps is visually represented in **Figure 2**. In the following section, a more detailed explanation of each step is provided.

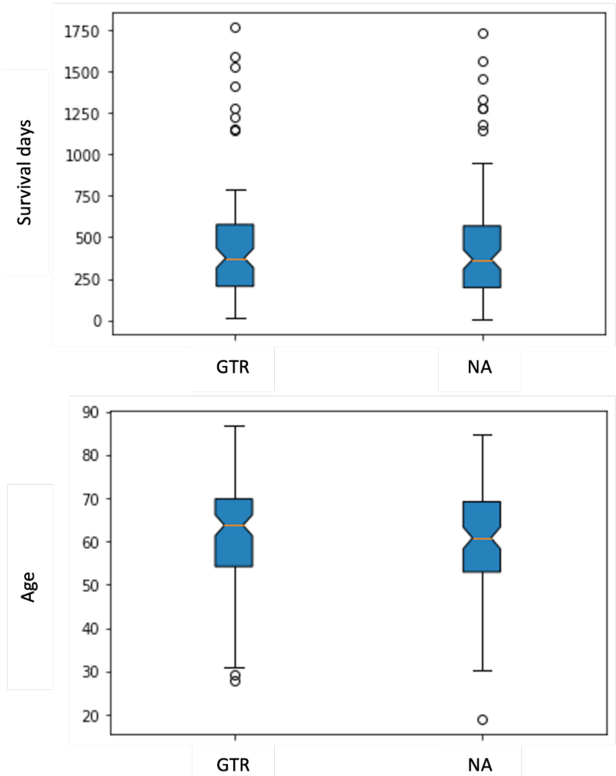

Figure 1. Distribution of age and survival days in patients with gross total resection status (GTR) and patients with unknown resection status (NA).

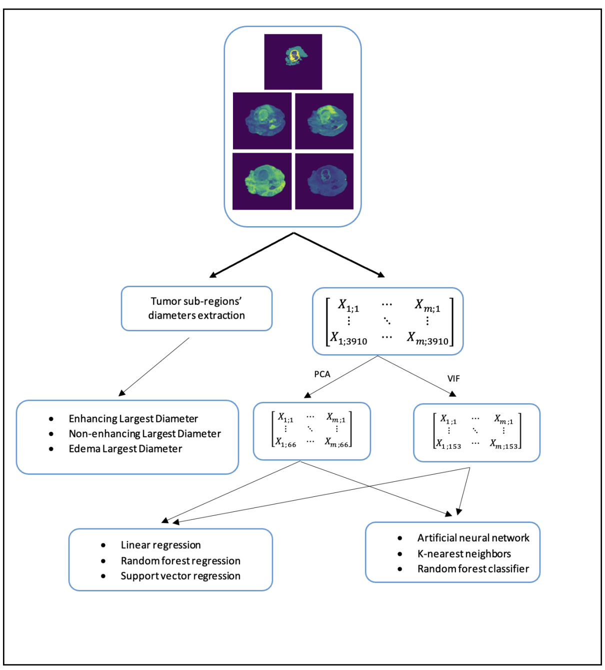

Figure 2. Methodology used to evaluate the predictiveness of location-based features independently and in combination with radiomics for overall survival.

3.1 Image preprocessing

Due to the limited dataset used in this study, it is necessary to normalize the images in order to reduce diversity and potential imaging errors. To achieve this, we followed the approach outlined in previous relevant studies and opted for N4 bias field correction and z-score normalization [36]. These techniques were employed to address differences in image intensities and ensure that the images are normalized in terms of both variance and zero mean.

- Z-score normalization: Z-score normalization, also known as standardization, is a technique used to normalize the pixel values of an image. It involves subtracting the mean value of the pixel intensities from each pixel and then dividing the result by the standard deviation of the pixel intensities. Mathematically, the z-score formula can be expressed as follows, where μ is the population mean, σ is the population standard deviation, and *x* is the individual data point being evaluated:

$$z = \frac{x - \mu}{\sigma}$$

z-score normalization

- N4 bias field correction: N4 bias field correction is a commonly used technique in medical image preprocessing. It involves employing a multi-scale optimization approach to estimate and correct for a smooth, slowly varying and multiplicative field present in the images. This correction helps address intensity variations caused by factors such as uneven illumination or magnetic field inhomogeneities. Gaillochet [37] demonstrated the effectiveness of N4 bias field correction in their research, supporting its usefulness as a preprocessing step in medical image analysis.

3.2 Radiomic feature extraction

To extract the radiomic features, we utilized the Pyradiomics module, as introduced by Griethuysen [38]. This module offers a comprehensive set of tools and algorithms specifically designed for radiomic feature extraction. The extracted features encompass various categories, including first-order statistics, shape-based features (both 3D and 2D), gray level co-occurrence matrix, gray level run length matrix, gray level size zone matrix, neighboring gray-tone difference matrix, and gray level dependence matrix. These features provide valuable information about the texture, shape, and spatial relationships within the medical images, enabling a more comprehensive characterization of the tumor sub-regions.

A total of 3910 features were extracted from the images, while there was a total of 201 patients with GTR and NA resection status. In order to prevent overfitting and enhance the efficiency of the modeling process, feature reduction algorithms, as described by Bzdok [39], were applied. These algorithms helped in selecting the most important features, reducing the dimensionality of the dataset, and mitigating the risk of overfitting.

3.3 Standardization and preselection of features

To ensure reliable predictive models and address variability, the radiomic features were initially standardized using the scikit-learn object StandardScaler to have a value between zero and one. Reducing the dimensionality of the features became necessary due to redundancy. Therefore, the correlation matrix was first applied, followed by the variance inflation factor (VIF) and principal component analysis (PCA) independently.

- Correlation Matrix: In this approach, a simple linear regression was performed between each individual feature and the others. The pairwise correlations were evaluated, and representative features were selected based on their correlations [40]. In the correlation matrix, areas with correlations above 95 percent were reduced to retain the most variable element.
- Variance Inflation Factor (VIF): The VIF preselection method was applied to the remaining features after the correlation matrix step to address multicollinearity. The commonly recommended threshold is 10, and features exhibiting a VIF exceeding this value were removed to address concerns related to collinearity.
- Principal Component Analysis (PCA): PCA was employed to extract essential information from the dataset [41] and reduce dimensionality [42]. After applying PCA to the features outputted from the correlation matrix, only the features capturing 95 percent of the variance in the data were retained for the subsequent learning process.

3.4 Statistical hypothesis testing

To assess the impact of individual features on OS prediction and control for false discoveries, hypothesis tests were deemed necessary. It is important to note that controlling the false discovery rate (FDR) on PCA-selected features is not required, as this algorithm selects the most relevant elements based on their association with OS. On the other hand, VIF eliminates features based on multicollinearity, with OS having no influence on the VIF selection process. Hence, the Benjamini-Hochberg procedure [43] was applied to the data remaining after VIF feature selection, using a specific level of $\alpha = 0.05$, to control the FDR and minimize the risk of false discoveries.

3.5 Tumor sub-regions' feature extraction

The primary objective of this study is to assess the predictive value of tumor sub-regions' maximum diameters on overall survival (OS) in patients with different resection statuses as it provides valuable information about the extent and size of the tumor sub-regions, which has significant implications for treatment planning and patient prognosis. To achieve this, the tumor sub-regions, including the enhancing tumor, non-enhancing necrotic tumor core, and edema, were segmented for each patient based on the labels available in the BraTS dataset. The Euclidean distance algorithm was utilized to calculate the largest diameter of the enhancing tumor, non-enhancing necrotic tumor core, and edema regions.

3.6 Prediction models

Regression and classification predictive models were utilized to assess the correlation between the maximum diameters of sub-regions and their survival outcomes, considering the patient's resection status. For the regression models, the maximum diameters of tumor sub-regions were directly fitted to the patients' survival days to predict the exact duration of survival. In contrast, the classification models aimed to classify patients into two main groups based on their survival days: short and medium survival (< 450 days) and extended survival (> 450 days). This approach provided a binary prediction of survival duration for the classification models.

Linear regression (LR), random forest regression (RFR), and support vector regression (SVR) models were employed to examine the univariate impact of maximum diameter features. The LR models indicate the linear relationship between two variables, with one as the explanatory variable and the other as the dependent variable. The RFR involves fitting multiple decision trees on different subsets of the dataset and averaging their predictions. The SVR is a nonparametric method that uses kernel functions to capture complex relationships between the features and the target variable.

For multivariate feature evaluation, the artificial neural network (ANN), random forest classifier (RFC), and k-nearest neighbors (KNN) models were selected. The ANN is designed to capture complex relationships between inputs and target values through interconnected nodes in different layers. The RFC combines the predictions of multiple decision trees to determine the final output. In the KNN algorithm, the new data point is assigned to the category of its closest neighbors based on similarity.

4. Results

In this section, the outcomes of the conducted research will be presented. This will include the results of the feature reductions applied to the extracted radiomic features, followed by the hypothesis testing of the VIF selected features. Furthermore, the robustness of the maximum diameters of tumor sub-regions is presented independently in univariate prediction models and in combination with the pre-selected radiomic features in multivariate prediction models.

4.1 Radiomic feature reduction approaches

First, following the approach described in Soltani [35], we employed a correlation matrix as the initial feature reduction algorithm, resulting in a reduction of radiomic features from 3910 to 1601. Subsequently, the VIF and PCA reduction methods were applied independently to the dataset selected by the correlation matrix. With the VIF selection method, the number of radiomic features was further reduced to 153 from the initial 1601. The PCA algorithm reduced the number of radiomic features from 1601 to 66.

4.2 Hypothesis testing

The Benjamini-Hochberg correction method was employed to select VIF features with the strongest correlation to patients' OS. Three features, namely *T2waveletHLL first order Skewness*, *T1waveletLHH first order Mean*, and *T2.log-sigma-3-0-mm 3D glszm Zone Percentage*, were chosen based on controlling the false discovery rate. These features were utilized in the LR model, and their correlation with OS was presented in **Table 1**. The p-values were calculated to determine the significance of the correlation between the selected VIF features and patients' OS using the linear correlation model. For the NA resection status, the selected features show similar values for MSE, RMSE, and Mean AE. However, the p-value indicates that *T1wavelet-LHH first order Mean* has the highest correlation, with the lowest value of 0.27. On the other hand, within the GTR dataset, *T2wavelet-HLL first order Skewness* feature has the lowest p-value of 0.159, indicating a strong correlation with OS.

4.3 Univariate prediction models

Table 2 presents the results of the regression models. The GTR dataset shows lower errors and better performance compared to the NA dataset. The average mean absolute error (MAE) and root mean squared error (RMSE) for the GTR dataset are 210 and 297, respectively. In contrast, the average MAE and RMSE for NA subjects are 242 and 315.

Spearman's correlation coefficients were also calculated. The majority of the coefficients are negative, indicating a strong correlation between higher tumor maximum diameters and lower survivals. For the GTR dataset, the correlation coefficient is approximately –0.08, while for the NA dataset, it is more decisive, with an average of –0.25. Comparing these results to **Table 1**, it becomes evident that the tumor sub-regions' maximum diameters have a greater impact on patients' OS than the selected VIF features.

The average p-values for sub-regions maximum diameters in the NA dataset are 0.035, significantly lower than the selected VIF features (0.436). Similarly, in the GTR dataset, the average p-values extracted from the linear regression for sub-regions' maximum diameters are 0.425, compared to 0.524 for VIF features. Similarly, MSE, RMSE, and MAE indicate a higher correlation of the newly extracted features compared to the nominated VIF features. The results of the linear regression model are visually depicted in **Figure 3**. **Figures 3a, 3b, and 3c** depict the Spearman correlation between the survival days of GTR patients and their respective non-enhancing tumor diameter, enhancing tumor diameter, and edema diameter. Similarly, **Figures 3d, 3e, and 3f** illustrate the Spearman correlation between the survival days of NA patients and their corresponding non-enhancing tumor diameter, enhancing tumor diameter, and edema diameter. The Spearman correlations, as presented in the subplots of **Figure 3**, along with the p-values from the regression models in **Table 2**, reveal that the diameters of tumor sub-

Table 1. Linear correlation analysis of VIF-selected features with overall survival.

Feature	Spearman R	MSE	RMSE	Mean AE	p value	Spearman R	MSE	RMSE	Mean AE	p value
	NA resection status					**GTR resection status**				
T2.wavelet HLL_ firstorder_Skewness	0.032	106745	326.71	264.25	0.622	0.129	62771	250.54	187.53	0.159
T1.wavelet-LHH_ firstorder_Mean	–0.109	103049	321.01	257.18	0.270	–0.005	58429	241.72	180.72	0.483
T2.log-sigma-3-0-mm-3D _glszm_ ZonePercentage	0.096	99680	315.72	259.00	0.417	0.128	59422	243.76	182.47	0.932

Table 2. Comparing regression model performance for various resection status types: D1 denotes the non-enhancing necrotic tumor core's diameter, D2 represents the enhancing tumor's diameter, and D3 indicates the edema's diameter.

Feature	Model	Spearman R	MSE	RMSE	Mean AE	p value	Model	Spearman R	MSE	RMSE	Mean AE	p value
	NA resection status						**GTR resection status**					
D_1	**LR**	–0.276	80414	283.57	232.37	0.012	LR	–0.076	63023	251.04	191.36	0.130
	RFR	–0.037	79671	282.26	221.38	0.278	RFR	0.302	71840	268.03	219.74	0.270
	SVR	0.050	93365	305.55	227.26	0.024	SVR	–0.210	65031	255.01	186.74	0.280
D_2	**LR**	–0.239	83991	289.81	233.59	0.085	LR	–0.085	73858	271.76	199.17	0.644
	RFR	–0.153	96529	310.69	260.66	0.517	RFR	–0.143	177719	421.568	267.20	0.545
	SVR	0.467	93155	305.21	227.24	0.037	SVR	–0.038	65190	255.32	186.88	0.870
D_3	**LR**	–0.248	98139	313.27	268.40	0.010	LR	–0.09	77189	277.83	200.31	0.502
	RFR	–0.056	127703	357.35	290.26	0.813	RFR	–0.157	182101	426.73	263.07	0.507
	SVR	0.416	153822	392.20	221.67	0.068	SVR	–0.20	65289	255.51	186.96	0.390

regions for NA patients exhibit a stronger correlation with survival days (average Spearman correlation of –0.3 and average p-value of 0.035) compared to GTR patients (average Spearman correlation of –0.12 and average p-value of 0.425).

4.4 Multivariate prediction models

To transform the survival outcomes into binary categories, a midpoint of 450 days was selected based on the suggestion from the BraTs challenge (considering long-survivors as those with survival times greater than 450 days and short-survivors as those with survival times less than 450 days). This choice offers an additional advantage since the dataset is already balanced, eliminating the need to address any potential issues related to imbalanced data.

The regression models highlight the effectiveness of tumor sub-regions' maximum diameters. In the classification methods (ANN, RFC, and KNN), the aim was to assess the robustness of the new features when combined with radiomics. The dataset was split into training, validation, and test sets (60% for training, 20% for validation, and 20% for testing). The results of the test set can be found in **Table 3** and **Table 4**.

Across most algorithms, the presence of tumor sub-regions' maximum diameters shows a positive impact on the prediction of OS. The inclusion of the features improved the accuracy and precision of the classification methods by approximately 5%. The highest performance is observed in PCA-selected features for GTR patients, achieving an accuracy of 80%. Furthermore, integrating radiomics with tumor sub-regions' maximum diameters noticeably improved the area under the curve (AUC) values. In the GTR dataset, the combination of VIF-selected features and the maximum diameters of tumor sub-regions achieved the highest AUC of 70%. When the sub-regions' maximum diameters were added to radiomics,

Table 3. Performance comparison of classification models for patients reported as gross total resection status (GTR).

Model	Accuracy	Precision	Sensitivity	Specificity	AUC	Model	Accuracy	Precision	Sensitivity	Specificity	AUC
VIF-based feature subset						**VIF-based feature subset and tumor sub-regions diameter**					
ANN	0.70	0.44	0.81	0.55	0.67	ANN	0.70	0.55	0.81	0.55	0.70
KNN	0.70	0.68	0.70	0.67	0.60	KNN	0.80	0.75	0.82	0.67	0.67
RFC	0.64	0.57	0.81	0.50	0.59	RFC	0.68	0.63	0.87	0.67	0.68
PCA-based feature subset						**PCA-based feature subset and tumor sub-regions diameter**					
ANN	0.65	0.76	0.71	0.50	0.60	ANN	0.69	0.69	0.75	0.50	0.63
KNN	0.60	0.44	0.66	0.71	0.60	KNN	0.75	0.78	0.72	0.78	0.62
RFC	0.64	0.55	0.70	0.40	0.54	RFC	0.64	0.82	0.61	0.42	0.56

Table 4. Performance comparison of classification models for patients reported as unknown resection status (NA).

Model	Accuracy	Precision	Sensitivity	Specificity	AUC	Model	Accuracy	Precision	Sensitivity	Specificity	AUC
VIF-based feature subset						**VIF-based feature subset and tumor sub-regions diameter**					
ANN	0.60	0.71	0.714	0.33	0.56	ANN	0.65	0.40	0.733	0.40	0.58
KNN	0.70	0.63	0.722	1.00	0.55	KNN	0.75	0.82	0.705	1.00	0.69
RFC	0.72	0.63	0.833	0.43	0.64	RFC	0.68	0.72	0.650	0.80	0.65
PCA-based feature subset						**PCA-based feature subset and tumor sub-regions diameter**					
ANN	0.60	0.89	0.533	0.80	0.61	ANN	0.65	0.71	0.769	0.43	0.63
KNN	0.65	0.82	0.631	0.79	0.56	KNN	0.80	0.86	0.737	0.86	0.60
RFC	0.68	0.60	0.695	0.50	0.53	RFC	0.68	0.62	0.714	0.50	0.57

the AUC values for ANN, KNN, and RFC methods increased with an average of 4.42%. Additionally, incorporating the new features led to a nearly 7% increase in AUC for VIF-based features in RFC and KNN methods specifically for the GTR dataset.

It is worth noting that certain algorithms in the study did not show significant improvements when incorporating the newly extracted features. Furthermore, the results did not emphasize the impact of resection status on enhancing survival prediction. These observations can be attributed to the limited dataset size utilized in the study.

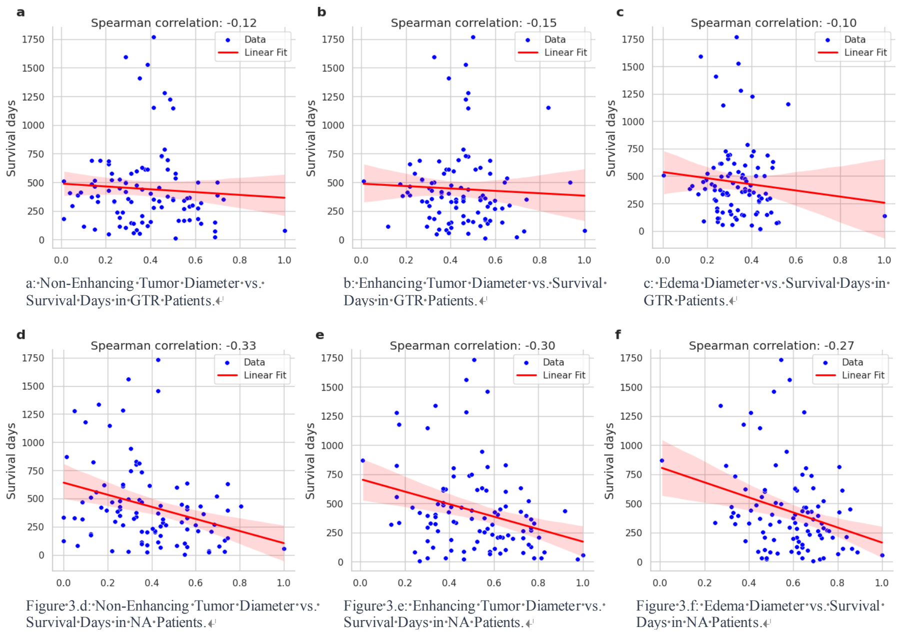

Figure 3. Scatter plot with linear regression line showing correlation between maximum diameter values (D1: non- enhancing tumor diameter, D2: enhancing tumor diameter, D3: edema diameter) and survival days, stratified by resection status. Graphs a, b, and c represent patients with GTR resection status, while graphs d, e, and f represent patients with NA resection status.

5. Discussion

In recent years, the use of machine learning in medical image analysis has been extensively explored in various studies. Many of these studies have focused on cancer datasets and utilized computer-aided learning algorithms. However, the resection status, which refers to the extent of surgical removal of the tumor, has often been overlooked [9].

In several previous research works, all types of resection status have been combined and used together in the learning algorithms [44–48]. Similarly, radiomics has been employed for quantitative analysis of MRI [49] and 3D deep feature learning [50] without specifically considering the resection status.

In our study, we examined the influence of resection status on regression and classification models. While certain learning algorithms exhibited improved performance when trained on specific resection statuses, the difference was not statistically significant in some cases. These findings suggest that resection status is a potentially important factor in learning algorithms, but a larger and more diverse dataset is required for a more comprehensive evaluation of its impact on survival prediction.

Radiomic features have been extensively employed in quantitative image analysis studies, and numerous research works have investigated their effectiveness. However, the reported accuracies in these studies have been limited. For instance, Sun [51] and Wijethilake [52] utilized radiomics in their image analysis studies but achieved learning accuracies below 70%. Similarly, Baid [53] employed a multi-layer perceptron (MLP) on radiomic features, resulting in an accuracy of 57.1% and a p-value of 0.427. In another study by Shaheen [54], region-specific radiomic features were the focus of their classification models, and they attained training and test set accuracies of 47.1% and 55.2%, respectively. In a study by Ammari [55], the entire BraTS dataset was used, incorporating all resection statuses in their predictive models. The AUC results for 9, 12, and 15 months were reported as 85%, 74%, and 58%, respectively. Furthermore, Calabrese [56] demonstrated that combining radiomics and deep learning features improves the accuracy of radiogenomic prediction for common glioblastoma genetic biomarkers compared to using either feature alone. In a recent study by Manjunath [57], radiomic features extracted from postcontrast T1-weighted (T1) images using 3D Slicer were employed for machine learning training. Among their evaluated models, the weighted subspace random forest exhibited the highest values for both the AUC and the concordance index (C-index), indicating its superior predictive performance for glioma patient survival. Chiesa [58] conducted a multicentric project, the GLIFA project, to investigate the role of radiomic analysis in guiding radiation target volume delineation for glioblastoma patients who have undergone total or near-total resection. This study aimed to personalize radiation treatment based on radiomic features extracted from the tissue around the resection cavity. The developed radiomic model was able to discriminate between patients with low-risk and high-risk relapse at 6 months with an AUC of 78.5%. Tran [59] focused on the prediction of survival of glioblastoma patients using local spatial relationships and global structure awareness in FLAIR MRI brain images, highlighting the utilization of radiomic features and machine learning models for survival prediction. The accuracy of the model is reported to be 0.621, and the Spearman's Rho is 0.576 in the validation set. Considering these findings, as well as our own study, it becomes evident that radiomic features alone may not be accurate enough for independent clinical applications especially for glioblastoma [60]. The tumor volumes and shape have shown great potential for the patients' OS cancer staging status. Here, we focused on the maximum diameters of tumor sub-regions. In binary OS classification models, the incorporation of additional features alongside radiomics yielded visible effects, suggesting that tumor sub-regions' maximum diameters can enhance the accuracy and improve the performance of the models. The regression models clearly showed the correlation between the maximum diameters of tumor sub-regions and patients' OS. The Benjamini-Hochberg algorithm identified three VIF-selected features that are highly relevant to OS. Notably, the correlation between the maximum diameters of tumor sub-regions and patients' OS is stronger than the correlation observed with the most correlated radiomic features selected using the VIF method. In contrast to Weninger's [9] research, where OS was categorized into three groups, we opted for a binary output in the classification algorithms due to its higher learning rates and accuracies. Adding tumor sub-regions' maximum diameters to radiomics improved the performance of the machine learning algorithms used in this study. This improvement has significant implications for developing better clinical treatment strategies and predicting cancer aggressiveness. To enhance the effectiveness of this approach, utilizing a broader and more diverse dataset is recommended. Therefore, radiomics should be considered an additional quantitative feature for improving the prediction of patients' OS.

Efforts have been made to utilize machine learning and imaging for the diagnosis and classification of cancer [61]. Quantitative imaging offers the potential to extract valuable features that may not be perceptible to clinicians. Therefore, combining essential medical imaging features identified by radiologists with quantitative medical imaging data can enhance the accuracy of evaluating the type and severity of cancer in patients.

Similar to previous studies, the achieved accuracies in both regression and classification models are not notably high, which can be attributed to the limitations of the dataset used. To overcome this issue, it is necessary to employ a larger and more comprehensive dataset, which would help address overfitting problems during training and validation. Moreover, the exploration and identification of novel imaging features, alongside radiomics, have the potential to enhance the predictive capabilities of OS and improve the precision and accuracy of learning algorithms. This, in turn, can facilitate their practical use in medical treatments.

6. Conclusions

In this study, we utilized the BraTS 2019 training dataset to investigate the relationship between the maximum diameters of tumor sub-regions and patients' OS. The regression models employed in our analysis revealed a clear correlation between the maximum diameters of tumor sub-regions and patients' OS. Additionally, we explored the effectiveness of integrating the newly extracted features with radiomics using classification models. Our findings demonstrated that the inclusion of tumor sub-regions' maximum diameters in the classification models yielded positive responses. This was observed in both the GTR and NA datasets, with an average increase of 4.58% in accuracy. The differences in results between the GTR and NA datasets in some of the machine learning algorithms further highlighted the resection status as a potentially important factor in the prediction models.

This study considered 450 days as the midpoint for survival days, leading to binary classification. However, utilizing a more extensive and diverse dataset with a broader class distribution would enable multiple classifications, providing a more accurate estimation of patients' survival rates and enhancing generalizability. Additionally, assessing additional features related to the medical characteristics of tumor regions would improve the interpretability of machine learning models, ensuring that these features hold tangible medical and clinical significance for validation. The models employed in this study exhibit computational efficiency, underscoring their inherent advantages. As we consider future directions, exploring alternative deep learning models, particularly transformer-based ones, and incorporating additional clinical and genetic data may demand increased computational resources. However, the potential for achieving superior results justifies the computational costs for advancing our understanding and applications in this domain. Also, a deeper investigation into the NA characteristics of resection status is recommended to enhance understanding and enable a robust comparison with GTA resection status.

Author Contributions

RB, AB, and NS preprocessed the data set, performed algorithm implementation, and wrote the manuscript. MS and KR supervised the work, read and edited the manuscript, and discussed the results. All authors contributed to the article and approved the submitted version.

Informed Consent

Ethical review and approval were not required for the study on human participants in accordance with the local legislation and institutional requirements. Written informed consent for participation was not required for this study in accordance with the national legislation and the institutional requirements.

Data Availability

Publicly available datasets were analyzed in this study. This data can be found here: https://www.med.upenn.edu/sbia/brats2018/registration.html.

Conflicts of Interest

The authors declare that the research was conducted in the absence of any commercial or financial relationships that could be construed as a potential conflict of interest.

References

[1] Garanti, T., Alhnan, M.A., Wan, K.W., 2021. The potential of nanotherapeutics to target brain tumors: Current challenges and future opportunities. Nanomedicine. 16(21), 1833–1837. DOI: https://doi.org/10.2217/nnm-2021-0134

[2] Goodenberger, M.L., Jenkins, R.B., 2012. Genetics of adult glioma. Cancer Genetics. 205(12), 613–621.
DOI: https://doi.org/10.1016/j.cancergen.2012.10.009

[3] Atkinson, M., Juhász, C., Shah, J., et al., 2008. Paradoxical imaging findings in cerebral gliomas. Journal of the Neurological Sciences. 269(1–2), 180–183.
DOI: https://doi.org/10.1016/j.jns.2007.12.029

[4] Wang, Y., Zhao, W., Xiao, Z., et al., 2020. A risk signature with four autophagy-related genes for predicting survival of glioblastoma multiforme. Journal of Cellular and Molecular Medicine. 24(7), 3807–3821.
DOI: https://doi.org/10.1111/jcmm.14938

[5] Holland, E.C., 2000. Glioblastoma multiforme: The terminator. Proceedings of the National Academy of Sciences. 97(12), 6242–6244.
DOI: https://doi.org/10.1073/pnas.97.12.6242

[6] Gomez, S.L., Shariff-Marco, S., DeRouen, M., et al., 2015. The impact of neighborhood social and built environment factors across the cancer continuum: Current research, methodological considerations, and future directions. Cancer. 121(14), 2314–2330.
DOI: https://doi.org/10.1002/cncr.29345

[7] McTiernan, A., Friedenreich, C.M., Katzmarzyk, P.T., et al., 2019. Physical activity in cancer prevention and survival: A systematic review. Medicine and Science in Sports and Exercise. 51(6), 1252–1261.
DOI: https://doi.org/10.1249/MSS.0000000000001937

[8] Carrera, P.M., Kantarjian, H.M., Blinder, V.S., 2018. The financial burden and distress of patients with cancer: Understanding and stepping-up action on the financial toxicity of cancer treatment. CA: A Cancer Journal for Clinicians. 68(2), 153–165.
DOI: https://doi.org/10.3322/caac.21443

[9] Weninger, L., Haarburger, C., Merhof, D., 2019. Robustness of radiomics for survival prediction of brain tumor patients depending on resection status. Frontiers in Computational Neuroscience. 13, 73.
DOI: https://doi.org/10.3389/fncom.2019.00073

[10] Jonklaas, J., Nogueras-Gonzalez, G., Munsell, M., et al., 2012. The impact of age and gender on papillary thyroid cancer survival. The Journal of Clinical Endocrinology & Metabolism. 97(6), E878–E887.
DOI: https://doi.org/10.1210/jc.2011-2864

[11] Chowdhary, C.L., Acharjya, D.P., 2020. Segmentation and feature extraction in medical imaging: A systematic review. Procedia Computer Science. 167, 26–36.
DOI: https://doi.org/10.1016/j.procs.2020.03.179

[12] Choi, Y., Nam, Y., Jang, J., et al., 2021. Radiomics may increase the prognostic value for survival in glioblastoma patients when combined with conventional clinical and genetic prognostic models. European Radiology. 31, 2084–2093.
DOI: https://doi.org/10.1007/s00330-020-07335-1

[13] Ardakani, A.A., Bureau, N.J., Ciaccio, E.J., et al., 2022. Interpretation of radiomics features—a pictorial review. Computer Methods and Programs in Biomedicine. 215, 106609.
DOI: https://doi.org/10.1016/j.cmpb.2021.106609

[14] Tomaszewski, M.R., Gillies, R.J., 2021. The biological meaning of radiomic features. Radiology. 298(3), 505–516.
DOI: https://doi.org/10.1148/radiol.2021202553

[15] Hooper, G.W., Ginat, D.T., 2023. MRI radiomics and potential applications to glioblastoma. Frontiers in Oncology. 13, 1134109.
DOI: https://doi.org/10.3389/fonc.2023.1134109

[16] Zhu, J., Ye, J., Dong, L., et al., 2023. Non-invasive prediction of overall survival time for glioblastoma multiforme patients based on multimodal MRI radiomics. International Journal of Imaging Systems and Technology. 33(4), 1261–1274.
DOI: https://doi.org/10.1002/ima.22869

[17] Li, Y., Bao, L., Yang, C., et al., 2023. A multi-

parameter radiomic model for accurate prognostic prediction of glioma. MedComm–Future Medicine. 2(2), e41.
DOI: https://doi.org/10.1002/mef2.41

[18] Shboul, Z.A., Vidyaratne, L., Alam, M., et al., 2018. Glioblastoma and survival prediction. Brainlesion: Glioma, multiple sclerosis, stroke and traumatic brain injuries. Springer International Publishing: Cham. pp. 358–368.
DOI: https://doi.org/10.1007/978-3-319-75238-9_31

[19] Feng, X., Tustison, N.J., Patel, S.H., et al., 2020. Brain tumor segmentation using an ensemble of 3d u-nets and overall survival prediction using radiomic features. Frontiers in Computational Neuroscience. 14, 25.
DOI: https://doi.org/10.3389/fncom.2020.00025

[20] Bakas, S., Reyes, M., Jakab, A., et al., 2018. Identifying the best machine learning algorithms for brain tumor segmentation, progression assessment, and overall survival prediction in the BRATS challenge. arXiv preprint arXiv:1811.02629.

[21] Baid, U., Talbar, S., Rane, S., et al., 2019. Deep learning radiomics algorithm for gliomas (drag) model: A novel approach using 3d unet based deep convolutional neural network for predicting survival in gliomas. Brainlesion: Glioma, multiple sclerosis, stroke and traumatic brain injuries. Springer International Publishing: Cham. pp. 369–379.
DOI: https://doi.org/10.1007/978-3-030-11726-9_33

[22] Jungo, A., McKinley, R., Meier, R., et al., 2018. Towards uncertainty-assisted brain tumor segmentation and survival prediction. Brainlesion: Glioma, multiple sclerosis, stroke and traumatic brain injuries. Springer International Publishing: Cham. pp. 474–485.
DOI: https://doi.org/10.1007/978-3-319-75238-9_40

[23] Puybareau, E., Tochon, G., Chazalon, J., et al., 2019. Segmentation of gliomas and prediction of patient overall survival: A simple and fast procedure. Brainlesion: Glioma, multiple sclerosis, stroke and traumatic brain injuries. Springer International Publishing: Cham. pp. 199–209.
DOI: https://doi.org/10.1007/978-3-030-11726-9_18

[24] Sun, L., Zhang, S., Luo, L., 2019. Tumor segmentation and survival prediction in glioma with deep learning. Brainlesion: Glioma, multiple sclerosis, stroke and traumatic brain injuries. Springer International Publishing: Cham. pp. 83–93.
DOI: https://doi.org/10.1007/978-3-030-11726-9_8

[25] Choi, Y.S., Ahn, S.S., Chang, J.H., et al., 2020. Machine learning and radiomic phenotyping of lower grade gliomas: Improving survival prediction. European Radiology. 30, 3834–3842.
DOI: https://doi.org/10.1007/s00330-020-06737-5

[26] Wankhede, D.S., Selvarani, R., 2022. Dynamic architecture based deep learning approach for glioblastoma brain tumor survival prediction. Neuroscience Informatics. 2(4), 100062.
DOI: https://doi.org/10.1016/j.neuri.2022.100062

[27] Hu, Z., Yang, Z., Zhang, H., et al., 2022. A deep learning model with radiomics analysis integration for glioblastoma post-resection survival prediction. arXiv preprint arXiv:2203.05891.

[28] Fang, L., Wang, X., 2022. Brain tumor segmentation based on the dual-path network of multi-modal MRI images. Pattern Recognition. 124, 108434.
DOI: https://doi.org/10.1016/j.patcog.2021.108434

[29] Liu, J., Li, M., Wang, J., et al., 2014. A survey of MRI-based brain tumor segmentation methods. Tsinghua Science and Technology. 19(6), 578–595.
DOI: https://doi.org/10.1109/TST.2014.6961028

[30] Senders, J.T., Staples, P., Mehrtash, A., et al.,

2020. An online calculator for the prediction of survival in glioblastoma patients using classical statistics and machine learning. Neurosurgery. 86(2), E184–E192.
DOI: https://doi.org/10.1093/neuros/nyz403

[31] Menze, B.H., Jakab, A., Bauer, S., et al., 2014. The multimodal brain tumor image segmentation benchmark (BRATS). IEEE Transactions on Medical Imaging. 34(10), 1993–2024.
DOI: https://doi.org/10.1109/TMI.2014.2377694

[32] Bakas, S., Akbari, H., Sotiras, A., et al., 2017. Advancing the cancer genome atlas glioma MRI collections with expert segmentation labels and radiomic features. Scientific Data. 4, 170117.
DOI: https://doi.org/10.1038/sdata.2017.117

[33] Segmentation Labels for the Pre-operative Scans of the TCGA-GBM Collection [Internet]. The Cancer Imaging Archive. Available from: https://doi.org/10.7937/K9/TCIA.2017.KLXWJJ1Q

[34] Segmentation Labels and Radiomic Features for the Pre-operative Scans of the TCGA-LGG Collection [Internet]. The Cancer Imaging Archive. Available from: https://doi.org/10.7937/K9/TCIA.2017.GJQ7R0EF

[35] Soltani, M., Bonakdar, A., Shakourifar, N., et al., 2021. Efficacy of location-based features for survival prediction of patients with glioblastoma depending on resection status. Frontiers in Oncology. 11, 661123.
DOI: https://doi.org/10.3389/fonc.2021.661123

[36] Tustison, N.J., Avants, B.B., Cook, P.A., et al., 2010. N4ITK: Improved N3 bias correction. IEEE Transactions on Medical Imaging. 29(6), 1310–1320.
DOI: https://doi.org/10.1109/TMI.2010.2046908

[37] Gaillochet, M., Tezcan, K.C., Konukoglu, E., 2020. Joint reconstruction and bias field correction for undersampled MR imaging. Medical image computing and computer-assisted intervention. Springer International Publishing: Cham. pp. 44–52.
DOI: https://doi.org/10.1007/978-3-030-59713-9_5

[38] Van Griethuysen, J.J., Fedorov, A., Parmar, C., et al., 2017. Computational radiomics system to decode the radiographic phenotype. Cancer Research. 77(21), e104–e107.
DOI: https://doi.org/10.1158/0008-5472.CAN-17-0339

[39] Bzdok, D., 2017. Classical statistics and statistical learning in imaging neuroscience. Frontiers in Neuroscience. 11, 543.
DOI: https://doi.org/10.3389/fnins.2017.00543

[40] Gillies, R.J., Kinahan, P.E., Hricak, H., 2016. Radiomics: Images are more than pictures, they are data. Radiology. 278(2), 563–577.
DOI: https://doi.org/10.1148/radiol.2015151169

[41] Abdi, H., Williams, L.J., 2010. Principal component analysis. Wiley Interdisciplinary Reviews: Computational Statistics. 2(4), 433–459.
DOI: http://dx.doi.org/10.1002/wics.101

[42] Kambhatla, N., Leen, T.K., 1997. Dimension reduction by local principal component analysis. Neural Computation. 9(7), 1493–1516.
DOI: https://doi.org/10.1162/neco.1997.9.7.1493

[43] Benjamini, Y., Hochberg, Y., 1995. Controlling the false discovery rate: A practical and powerful approach to multiple testing. Journal of the Royal Statistical Society: Series B (Methodological). 57(1), 289–300.
DOI: https://doi.org/10.1111/j.2517-6161.1995.tb02031.x

[44] Gutman, D.A., Cooper, L.A., Hwang, S.N., et al., 2013. MR imaging predictors of molecular profile and survival: Multi-institutional study of the TCGA glioblastoma data set. Radiology. 267(2), 560–569.
DOI: https://doi.org/10.1148/radiol.13120118

[45] Macyszyn, L., Akbari, H., Pisapia, J.M., et al., 2015. Imaging patterns predict patient survival and molecular subtype in glioblastoma via machine learning techniques. Neuro-oncology. 18(3), 417–425.
DOI: https://doi.org/10.1093/neuonc/nov127

[46] Kickingereder, P., Burth, S., Wick, A., et al., 2016. Radiomic profiling of glioblastoma:

Identifying an imaging predictor of patient survival with improved performance over established clinical and radiologic risk models. Radiology. 280(3), 880–889.
DOI: https://doi.org/10.1148/radiol.2016160845

[47] Lao, J., Chen, Y., Li, Z.C., et al., 2017. A deep learning-based radiomics model for prediction of survival in glioblastoma multiforme. Scientific Reports. 7, 10353.
DOI: https://doi.org/10.1038/s41598-017-10649-8

[48] Li, Q., Bai, H., Chen, Y., et al., 2017. A fully-automatic multiparametric radiomics model: towards reproducible and prognostic imaging signature for prediction of overall survival in glioblastoma multiforme. Scientific Reports. 7, 14331.
DOI: https://doi.org/10.1038/s41598-017-14753-7

[49] Zhang, Z., Jiang, H., Chen, X., et al., 2014. Identifying the survival subtypes of glioblastoma by quantitative volumetric analysis of MRI. Journal of Neuro-oncology. 119, 207–214.
DOI: https://doi.org/10.1007/s11060-014-1478-2

[50] Nie, D., Zhang, H., Adeli, E., et al., 2016. 3D deep learning for multi-modal imaging-guided survival time prediction of brain tumor patients. Medical image computing and computer-assisted intervention. Springer International Publishing: Cham. pp. 212–220.
DOI: https://doi.org/10.1007/978-3-319-46723-8_25

[51] Sun, W., Jiang, M., Dang, J., et al., 2018. Effect of machine learning methods on predicting NSCLC overall survival time based on Radiomics analysis. Radiation Oncology. 13, 197.
DOI: https://doi.org/10.1186/s13014-018-1140-9

[52] Wijethilake, N., Islam, M., Ren, H., 2020. Radiogenomics model for overall survival prediction of glioblastoma. Medical & Biological Engineering & Computing. 58, 1767–1777.
DOI: https://doi.org/10.1007/s11517-020-02179-9

[53] Baid, U., Rane, S.U., Talbar, S., et al., 2020. Overall survival prediction in glioblastoma with radiomic features using machine learning. Frontiers in Computational Neuroscience. 14, 61.
DOI: https://doi.org/10.3389/fncom.2020.00061

[54] Shaheen, A., Burigat, S., Bagci, U., et al., 2020. Overall survival prediction in gliomas using region-specific radiomic features. Machine learning in clinical neuroimaging and radiogenomics in neuro-oncology. Springer International Publishing: Cham. pp. 259–267.
DOI: https://doi.org/10.1007/978-3-030-66843-3_25

[55] Ammari, S., Sallé de Chou, R., Balleyguier, C., et al., 2021. A predictive clinical-radiomics nomogram for survival prediction of glioblastoma using MRI. Diagnostics. 11(11), 2043.
DOI: https://doi.org/10.3390/diagnostics11112043

[56] Calabrese, E., Rudie, J.D., Rauschecker, A.M., et al., 2022. Combining radiomics and deep convolutional neural network features from preoperative MRI for predicting clinically relevant genetic biomarkers in glioblastoma. Neuro-Oncology Advances. 4(1), vdac060.
DOI: https://doi.org/10.1093/noajnl/vdac060

[57] Manjunath, M., Saravanakumar, S., Kiran, S., et al., 2023. A comparison of machine learning models for survival prediction of patients with glioma using radiomic features from MRI scans. Indian Journal of Radiology and Imaging. 33(3), 338–343.
DOI: https://doi.org/10.1055/s-0043-1767786

[58] Chiesa, S., Russo, R., Beghella Bartoli, F., et al., 2023. MRI-derived radiomics to guide post-operative management of glioblastoma: Implication for personalized radiation treatment volume delineation. Frontiers in Medicine. 10, 1059712.
DOI: https://doi.org/10.3389/fmed.2023.1059712

[59] Tran, M.T., Yang, H.J., Kim, S.H., et al., 2023. Prediction of survival of glioblastoma patients using local spatial relationships and global

structure awareness in FLAIR MRI brain images. IEEE Access. 11, 37437–37449.
DOI: https://doi.org/10.1109/ACCESS.2023.3266771

[60] Martin, P., Holloway, L., Metcalfe, P., et al., 2022. Challenges in glioblastoma radiomics and the path to clinical implementation. Cancers. 14(16), 3897.
DOI: https://doi.org/10.3390/cancers14163897

[61] Khan, M.A., Ashraf, I., Alhaisoni, M., et al., 2020. Multimodal brain tumor classification using deep learning and robust feature selection: A machine learning application for radiologists. Diagnostics. 10(8), 565.
DOI: https://doi.org/10.3390/diagnostics10080565

BILINGUAL PUBLISHING GROUP

Tel:+65 65881289
E-mail: contact@bilpublishing.com
Website:https://journals.bilpubgroup.com

2661-3204